JAERI - M
89-050

CONFINEMENT PROPERTIES OF PELLET INJECTED JT-60 PLASMAS

May 1989

Yutaka KAMADA, Ryuji YOSHINO, Masayuki NAGAMI
Takahisa OZEKI, Kouzo KAWASAKI, Hajime HIRATSUKA
Yasuhiko MIYO, Haruyuki KIMURA, Takeo NISHITANI
Hidetoshi YOSHIDA and Keisuke NAGASHIMA

日 本 原 子 力 研 究 所
Japan Atomic Energy Research Institute

JAERI-Mレポートは，日本原子力研究所が不定期に公刊している研究報告書です。
入手の問合わせは，日本原子力研究所技術情報部情報資料課（〒319-11茨城県那珂郡東海村）あて，お申しこしください。なお，このほかに財団法人原子力弘済会資料センター（〒319-11 茨城県那珂郡東海村日本原子力研究所内）で複写による実費頒布をおこなっております。

JAERI-M reports are issued irregularly.
Inquiries about availability of the reports should be addressed to Information Division, Department of Technical Information, Japan Atomic Energy Research Institute, Tokai-mura, Naka-gun, Ibaraki-ken 319-11, Japan.

編集兼発行　日本原子力研究所
印　　刷　㈱原子力資料サービス

JAERI-M 89-050

Confinement Properties of Pellet Injected JT-60 Plasmas

Yutaka KAMADA, Ryuji YOSHINO, Masayuki NAGAMI
Takahisa OZEKI, Kouzo KAWASAKI, Hajime HIRATSUKA
Yasuhiko MIYO, Haruyuki KIMURA, Takeo NISHITANI
Hidetoshi YOSHIDA and Keisuke NAGASHIMA

Department of Large Tokamak Research・Department of JT-60 Facility
Naka Fusion Research Establishment
Japan Atomic Energy Research Institute
Naka-machi, Naka-gun, Ibaraki-ken

(Received April 5, 1989)

Improved energy confinement for additionally heated JT-60 limiter and lower x-point discharges have been obtained with hydrogen pellet injection. Energy confinement time was enhanced up to 40% relative to usual gas fuelled discharges at the medium NB or NB+ICRF heating power for which the strongly peaked electron density profile was sustained within 0.5 sec after a series of pellet injection. The improved discharges are characterized by the pressure profile strongly peaked around the magnetic axis and degraded when a large sawtooth reappears or the pressure gradient may reach a critical value.

Keywords: Tokamak, Pellet Injection, Confinement, Pressure Gradient, NBI, JT-60

JT－60ペレット入射実験に於ける閉じ込め特性

日本原子力研究所那珂研究所
臨界プラズマ研究部・JT－60試験部
鎌田　裕・芳野　隆治・永見　正幸・小関　隆久
川崎　幸三・平塚　一・三代　康彦・木村　晴行
西谷　健夫・吉田　英俊・永島　圭介

（1989年4月5日受理）

JT－60の追加熱されたリミター及び下X点配位に於て，水素ペレット入射時に顕著な閉じ込め改善が見られた。エネルギー閉じ込め時間の改善は通常のガスパフ時に比べて最大40%である。改善度が最も高いのは中程度（＜15MW）の加熱（NBまたはNB＋ICRF）パワーであり，中心電子密度を$n_e(0)$，体積平均電子密度を$\langle n_e \rangle$とすると$n_e(0) < 2.0 \times 10^{20}\ m^{-3}$，$n_e(0)/\langle n_e \rangle < 5$という大きくピーキングした密度分布がペレット入射後0.5秒程度維持されている。また，プラズマ電流2.5MA時に得られた$n_e(0)\ T_e(0)\ \tau_E$は$6.8 \times 10^{19}\ m^{-3}$ keV secであり，従来3.1MAで得られていた値を越えている。閉じ込め改善は，プラズマ中心部（sawtooth反転半径の内側）で強くピーキングした圧力分布によって担われており，large sawtoothの出現あるいは圧力勾配が，ある上限値に達した場合にその上限が規定される。この圧力分布ピーキングは，ペレットの侵入距離に大きく依存する。下X点配位では，低q（$q < 3$）時に特に閉じ込め改善が顕著であるが，これはsawtoothの安定化によると考えられる。

那珂研究所：〒311－01　茨城県那珂郡那珂町大字向山801－1

Contents

目　　次

1. INTRODUCTION

Pellet fuelling experiments on many tokamaks have demonstrated its advantages of enhanced energy confinement in addition to the high fuelling efficiency relative to the usual gas puffing. After pioneering studies on ISX-A and -B [1,2], the enhanced confinement characteristics mainly due to the strongly peaked density profile have been observed on medium sized tokamaks viz. ALCATOR-C [3], D-III [4], ASDEX [5,6], JFT-2M [7] etc. The experimental observation in ALCATOR-C high-field ohmically heated (OH) discharges [3] had large impact on the fusion research: The global energy confinement time, τ_E, increased with electron density, n_e, in a high-n_e range and achieved Lawson number, $n_e\tau_E$, exceeded that required for the thermal break-even. In those tokamaks, the enhanced performance due to the pellet injection has also been observed for additionally heated discharges [4,6,7]. The improvements are related to reduction in the ion transport loss [6,8]. On the two large tokamaks, TFTR and JET, pellet injection experiments started and the obtained plasma performance turned out to be desirable. Such good results are owing to recent advances in injector technique producing high speed (>1.5km/sec) and/or multiple pellets which enables deep penetration into large and high temperature plasmas [9,10]. In TFTR OH experiments, the achieved Lawson number exceeded $1.4\times10^{20}m^{-3}sec$ [11]. In JET ICRF (+NB) heated limiter discharges, the fusion products of $1\sim2\times10^{20}m^{-3}keVsec$ comparable to the top data of H-mode were obtained [12,13]. The high performance of additionally heated plasmas in JET depends mainly on increase in density and the highly peaked temperature profile. The improvement in τ_E, however, is limited by up to 20%.

In JT-60, the pellet injection experiments started in June 1988. Since then, the plasma behavior of pellet fuelled limiter and lower-x point [14] discharges have been studied. A combination with neutral beam (NB) heating increased τ_E by 40% as compared to gas fuelled NB heated discharges. This paper presenting the results of the improved confinement characteristics of the hydrogen pellet injection experiments for JT-60 hydrogen plasmas is arranged as follows: In Sec.2, the experimental set-up of the pellet injector is described. Section 3 deals with parameters of target plasmas and the operation scenario of

the injection experiments. The enhanced characteristics are given in Sec.4. In Sec.5, the limit of the improved confinement is discussed. Section 6 summarizes the conclusion.

2. EXPERIMENTAL SET-UP

A four-barrel pneumatic pellet injector installed on JT-60 in March 1988 produces cylinder-shaped hydrogen pellets with velocities approaching 1.6km/sec, with which two small and two large pellets can be fired independently with time intervals of from 0.0 to 2.0 sec[15]. Sizes of the pellets are 2.7mmϕ(in diameter) ×2.7mm^{l} (in length) and 3.8mmϕ×3.8mm^{l}. The small and large pellets contain 0.7×10^{21} and 2.0×10^{21} atoms, respectively, which correspond to volume averaged electron density $\langle n_e \rangle$ of $1.7\times10^{19}m^{-3}$ and $4.9\times10^{19}m^{-3}$ in the typical JT-60 lower-x point configuration (R~3.00m, a~0.7m, V~40m^3). The averaged fuelling efficiency for the injector is typically 70~80% of the particle inventory determined by the ideal pellet dimensions and the remaining particles are lost in the formation and acceleration phases. The ablation profiles of injected pellets are monitored by a 7-channel H_α detector array using fiber optics with time response of 1μsec [16]. The line of sight of each detector, the geometry of the pellet injector, chords of a Thomson scattering system and a FIR interferometer are shown in Fig.1 for the lower x-point configuration. The pellets are injected with an angle of 47 degree from the midplane. The injection trajectory is off-axis and the nearest distance from the geometric center of the torus is 12cm. Figure 2 shows the magnetic surfaces of the limiter configuration and lines of sight of a lower half set of soft X-ray (SX) detectors (PIN diode array).

3. TARGET PLASMAS AND OPTIMIZATION OF THE OPERATION SCENARIO

The targets for the pellet experiments were OH or low-power NB heated (<2MW) plasmas with B_t=4.3~4.8T, I_p=1.5~2.5MA(limiter)/ 1.5~1.8MA(divertor), q_a=4.4~2.9(limiter)/ q_{eff}=3.5~2.8(divertor), $T_e(0)$= 2~3keV and $\bar{n}_e=2\sim3\times10^{19}m^{-3}$. The strongly peaked density profiles desirable for the heating experiments were obtainable only by the pellet penetration to or beyond the magnetic axis. Such penetration was achieved by a

the injection experiments. The enhanced characteristics are given in Sec.4. In Sec.5, the limit of the improved confinement is discussed. Section 6 summarizes the conclusion.

2. EXPERIMENTAL SET-UP

A four-barrel pneumatic pellet injector installed on JT-60 in March 1988 produces cylinder-shaped hydrogen pellets with velocities approaching 1.6km/sec, with which two small and two large pellets can be fired independently with time intervals of from 0.0 to 2.0 sec[15]. Sizes of the pellets are 2.7mmϕ(in diameter) ×2.7mm^{l} (in length) and 3.8mmϕ×3.8mm^{l}. The small and large pellets contain 0.7×10^{21} and 2.0×10^{21} atoms, respectively, which correspond to volume averaged electron density $\langle n_e \rangle$ of 1.7×10^{19}m^{-3} and 4.9×10^{19}m^{-3} in the typical JT-60 lower-x point configuration (R~3.00m, a~0.7m, V~40m^3). The averaged fuelling efficiency for the injector is typically 70~80% of the particle inventory determined by the ideal pellet dimensions and the remaining particles are lost in the formation and acceleration phases. The ablation profiles of injected pellets are monitored by a 7-channel Hα detector array using fiber optics with time response of 1μsec [16]. The line of sight of each detector, the geometry of the pellet injector, chords of a Thomson scattering system and a FIR interferometer are shown in Fig.1 for the lower x-point configuration. The pellets are injected with an angle of 47 degree from the midplane. The injection trajectory is off-axis and the nearest distance from the geometric center of the torus is 12cm. Figure 2 shows the magnetic surfaces of the limiter configuration and lines of sight of a lower half set of soft X-ray (SX) detectors (PIN diode array).

3. TARGET PLASMAS AND OPTIMIZATION OF THE OPERATION SCENARIO

The targets for the pellet experiments were OH or low-power NB heated (<2MW) plasmas with B_t=4.3~4.8T, I_p=1.5~2.5MA(limiter)/ 1.5~1.8MA(divertor), q_a=4.4~2.9(limiter)/ q_{eff}=3.5~2.8(divertor), $T_e(0)$= 2~3keV and $\bar{n}_e=2\sim3\times10^{19}$m^{-3}. The strongly peaked density profiles desirable for the heating experiments were obtainable only by the pellet penetration to or beyond the magnetic axis. Such penetration was achieved by a

the injection experiments. The enhanced characteristics are given in Sec.4. In Sec.5, the limit of the improved confinement is discussed. Section 6 summarizes the conclusion.

2. EXPERIMENTAL SET-UP

A four-barrel pneumatic pellet injector installed on JT-60 in March 1988 produces cylinder-shaped hydrogen pellets with velocities approaching 1.6km/sec, with which two small and two large pellets can be fired independently with time intervals of from 0.0 to 2.0 sec[15]. Sizes of the pellets are 2.7mm$^{\phi}$(in diameter) ×2.7mm^{l} (in length) and 3.8mm$^{\phi}$×3.8mm^{l}. The small and large pellets contain 0.7×10^{21} and 2.0×10^{21} atoms, respectively, which correspond to volume averaged electron density $\langle n_e \rangle$ of $1.7\times10^{19}m^{-3}$ and $4.9\times10^{19}m^{-3}$ in the typical JT-60 lower-x point configuration (R~3.00m, a~0.7m, V~40m^3). The averaged fuelling efficiency for the injector is typically 70~80% of the particle inventory determined by the ideal pellet dimensions and the remaining particles are lost in the formation and acceleration phases. The ablation profiles of injected pellets are monitored by a 7-channel H_α detector array using fiber optics with time response of 1μsec [16]. The line of sight of each detector, the geometry of the pellet injector, chords of a Thomson scattering system and a FIR interferometer are shown in Fig.1 for the lower x-point configuration. The pellets are injected with an angle of 47 degree from the midplane. The injection trajectory is off-axis and the nearest distance from the geometric center of the torus is 12cm. Figure 2 shows the magnetic surfaces of the limiter configuration and lines of sight of a lower half set of soft X-ray (SX) detectors (PIN diode array).

3. TARGET PLASMAS AND OPTIMIZATION OF THE OPERATION SCENARIO

The targets for the pellet experiments were OH or low-power NB heated (<2MW) plasmas with B_t=4.3~4.8T, I_p=1.5~2.5MA(limiter)/ 1.5~1.8MA(divertor), q_a=4.4~2.9(limiter)/ q_{eff}=3.5~2.8(divertor), $T_e(0)$= 2~3keV and $\bar{n}_e=2\sim3\times10^{19}m^{-3}$. The strongly peaked density profiles desirable for the heating experiments were obtainable only by the pellet penetration to or beyond the magnetic axis. Such penetration was achieved by a

combination of one or two 2.7mmϕ and a 3mmϕ pellets. To find out the optimum scenario of pellet injection, plasma density just before the injection was scanned in a series of 1.5MA ohmically heated lower-x point discharges [17] : For low density ($\bar{n}_e \lesssim 2\times10^{19}m^{-3}$), the pellet penetration was limited at the periphery because of high temperature and probably the ablation due to high energy electrons. In such cases decay time of $\bar{n}_e$ after the pellet injection was short. For high density ($\bar{n}_e \gtrsim 3\times10^{19}m^{-3}$), pellet hit the inner side wall passing through the plasma because of low electron temperature and the radiated power loss increased rapidly.due to the deterioration of the power balance in the periphery In this case the plasma became disruptive and the stored energy decreased or the discharge terminated by a major disruption. The inner half region of the plasma has been already cooled before the pellet penetrate beyond the axis because the plasma particles diffuse along the field lines faster than the pellet speed, therefore, the ablation rate decreases drastically at r<0 and the pellet can reach the inner side wall. For medium density ($\bar{n}_e$~2~3$\times10^{19}m^{-3}$), pellets penetrated near the axis, the radiated power was small and increase in the stored energy had the maximum value. In this case the decay time of $\bar{n}_e$ reached 1~1.5sec. These experimental results show that the control of target plasma density is important for the optimum pellet penetration, which depends also on number and time interval of pellets, plasma current and the configuration of the plasma. The window of the optimum density is small and the achieved density alters with the wall condition (JT-60 uses carbon tiles for the first wall). To enlarge the optimum window, we adopted an operation scenario shown in Fig.3 (a). The typically adopted time interval of each pellet is 50 msec and the pellets are injected into low-power (~1.7MW ; 1unit of NBI) NB heated plasmas. In this case the plasma is stable even when the pellet penetrate beyond the axis, because the remaining mass of the pellet at r<0 can be evaporated due to the NB power and stable penetration is obtained. In the heating experiments, main heating powers were injected just after the last pellet. This is because , if the main power is applied before the pellet injection, pellets cannot penetrate to the center of hot plasmas and because NB injection into the peaked density profile produced by pellets can make power deposition profile peaked around the axis.Figure 3(b) shows ablation profiles of the three pellets for a lower x-point 1.8MA discharge (E8007). The first and the

second pellets reach r=0.45 and r=0.25m, respectively, and the last pellet penetrates beyond the axis. The ablation profiles measured are in good agreement with results calculated with a pellet ablation code based on the Parks-Turnbull's model [18] and the large dip on the third profile at r~20cm corresponds to the position of the q=1 resonant surface [16]. JT-60 has 14 unit NBI systems with an injected power level of ~1.7MW/unit and 14 steps of NB power can be utilized in the heating experiment. When two units were adopted for the bias injection (~3.4MW), it was hard to penetrate the pellets deeply into the plasma or the resultant n_e profiles became broad and increase in the stored energy was small. Figure 4 shows achieved electron density and temperature profiles measured with the Thomson scattering system and the power deposition profiles for a NB heated 2.1MA limiter discharge with P_{abs} of 5.4MW at 0.4 sec after a series of three pellets when the stored energy measured with a diamagnetic loop (W^{DIA}) reaches the maximum value. The density profile has a peaking factor, $n_e(0)/\langle n_e \rangle$, of ~5 with the central value $n_{e(0)} \sim 1.8\times10^{20}m^{-3}$. The power deposition profiles were calculated with an orbit following monte-carlo code OFMC [19]. The vertically injected hydrogen neutral beam with energy of 70keV has a diameter of ~40cm and the centrally peaked power deposition profile can be produced in the pellet fuelled conditions. There remains, however, ambiguities for central values, since the Thomson scattering measurement does not cover the central region within r<20cm.

4. IMPROVED PERFORMANCE OF PELLET FUELLED PLASMAS

4.1 Lower X-point Discharges

Figure 5 shows the relationship between the plasma stored energy W^{DIA} and the absorbed power P_{abs} for NB heated 1.8MA (a) and 1.5MA (b) lower x-point discharges. The open circles correspond to data of pellet fuelled discharges. The gas fuelled discharges at P_{abs}<13MW were operated to have high-$\bar{n}_e$ of $\sim5\times10^{19}m^{-3}$ which was comparable to the pellet data. The phenomenological findings demonstrated by Fig.5 are as follows: The improvement in W^{DIA} due to the pellet injection has the maximum value at medium P_{abs} of ~10MW and reduces asymptotically to the base (gas fuelled) value at P_{abs}>15MW. The

second pellets reach r=0.45 and r=0.25m, respectively, and the last pellet penetrates beyond the axis. The ablation profiles measured are in good agreement with results calculated with a pellet ablation code based on the Parks-Turnbull's model [18] and the large dip on the third profile at r~20cm corresponds to the position of the q=1 resonant surface [16]. JT-60 has 14 unit NBI systems with an injected power level of ~1.7MW/unit and 14 steps of NB power can be utilized in the heating experiment. When two units were adopted for the bias injection (~3.4MW), it was hard to penetrate the pellets deeply into the plasma or the resultant n_e profiles became broad and increase in the stored energy was small. Figure 4 shows achieved electron density and temperature profiles measured with the Thomson scattering system and the power deposition profiles for a NB heated 2.1MA limiter discharge with P_{abs} of 5.4MW at 0.4 sec after a series of three pellets when the stored energy measured with a diamagnetic loop (W^{DIA}) reaches the maximum value. The density profile has a peaking factor, $n_e(0)/\langle n_e \rangle$, of ~5 with the central value $n_{e(0)}$~$1.8\times10^{20}m^{-3}$. The power deposition profiles were calculated with an orbit following monte-carlo code OFMC [19]. The vertically injected hydrogen neutral beam with energy of 70keV has a diameter of ~40cm and the centrally peaked power deposition profile can be produced in the pellet fuelled conditions. There remains, however, ambiguities for central values, since the Thomson scattering measurement does not cover the central region within r<20cm.

4. IMPROVED PERFORMANCE OF PELLET FUELLED PLASMAS

4.1 Lower X-point Discharges

Figure 5 shows the relationship between the plasma stored energy W^{DIA} and the absorbed power P_{abs} for NB heated 1.8MA (a) and 1.5MA (b) lower x-point discharges. The open circles correspond to data of pellet fuelled discharges. The gas fuelled discharges at P_{abs}<13MW were operated to have high-$\bar{n}_e$ of ~$5\times10^{19}m^{-3}$ which was comparable to the pellet data. The phenomenological findings demonstrated by Fig.5 are as follows: The improvement in W^{DIA} due to the pellet injection has the maximum value at medium P_{abs} of ~10MW and reduces asymptotically to the base (gas fuelled) value at P_{abs}>15MW. The

increase in W^{DIA} at high P_{abs} is larger in 1.8MA discharges than in 1.5MA cases, which implies the confinement can be improved by higher P_{abs} at higher plasma current. In Fig.5(a), the improvement in W^{DIA} or τ_E for the pellet data is up to 40% compared to the base line at P_{abs} of 9.5MW. In this paper τ_E is calculated with values at the flat top of the stored energy and contribution of dW/dt is negligible. Figures 6, 7 and 8 show the comparison of plasma parameters among gas fuelled (E8009), two-pellet (E8005) and three-pellet injected (E8007) discharges at the same P_{abs} of 9.5MW. The operational sequence and the pellet ablation profiles for E8007 have been shown in Fig.3. In Fig.6, sets of traces for the three discharges are presented. For E8007, the line density averaged at r=0.7a increases immediately up to $6\times10^{19}m^{-3}$, then decays slowly to the gas-fuelled level and the central electron temperature, $T_e(0)$, measured by ECE emission decreases as the discharge is diluted by cold particles from the pellet, then, recovers with a time scale similar to the decay of $\bar{n}_e$. The stored energy for E8007 takes the maximum value at t=6.2 sec when $T_e(0)$ almost recovers to its initial value and happens to decay simultaneously with the onset of a large sawtooth (shown later in Fig. 8). For E8005, $\bar{n}_e$(r=0.7a) just after the pellet injection is higher than that for E8007, however decays faster. This means the pellet does not penetrate deeply into the core region. In Fig.7, profiles of n_e and T_e for the three discharges measured at t=6.2sec (0.4 sec after the pellet injection) with the Thomson scattering system. The T_e profiles for E8007 and E8005 have almost the same values with that for E8009, while $n_e(r)$ for the pellet discharges are kept much higher than that for the gas fuelled shot especially in the core region. Therefore the increase in the stored energy is concluded to depend mainly on the increase in the density. Figure 8 presents signal intensities of the soft-X ray emitted from the core region ; (a) and (b) show time evolutions of spatial distribution and those for the 4 chords near the magnetic axis, respectively.The SX profile for E8007 peaks strongly in a region inside Ch.10 for E8007. In turn, for E8005, the profile is flat in this region. For E8007 a small sawtooth is observed at t=6.04 sec, for E8005 repeating sawteeth occur from t=6.0 sec. Their inversion radii correspond to the position of the Ch.10. The stored energy of E8005 (Fig.6) saturates simultaneously with the onset of the first sawtooth at t=6.0 sec, and that of E8007 happens to decrease at t=6.2

sec also with the onset of the large sawtooth. From these observations, the SX profiles strongly peaked inside the sawtooth inversion radii (r_s) after the pellet injection are the key features of improved confinement characteristics of NB heated discharges.

The energy confinement time τ_E for the pellet and gas fuelled discharges with B_t=4.5T are plotted in Fig.9 as a function of the plasma current I_p. For the gas fuelled lower-x point discharges, the increase in τ_E with I_p is degraded at q_{eff}<3 [20]. While, for the pellet discharges, τ_E increases linearly with I_p at q_{eff}<3 and the improvement due to the pellet injection is distinct in the low-q regime (I_p=1.8MA) probably due to suppression of the sawtooth activity.

The peaked SX profiles has not been produced for ohmically heated pellet discharges so far. The time evolution of the SX profile is shown in Fig.10 for a 1.5MA lower x-point discharge E7471. In this case three pellets were injected from t=4.9 to 5.0 sec with time intervals of 50msec. The difference in the SX profile between OH and NB heated discharges can be related to the differences in the heating power deposition profiles. For E7471, the maximum W^{DIA} was also limited by an occurrence of a large sawtooth at t=5.4sec, the stored energy was, however, degraded smoothly to the gas fuelled level. This is because the improvement in W^{DIA} for OH discharges are sustained in whole region of the plasma. The sawteeth oscillations after the pellet injection had large amplitude and long period of ~100msec which is longer than that before the injection by a factor of 2~3.

4.2 Limiter discharges

Figure 11 shows the relationship between W^{DIA} and P_{abs} for NB heated 2.1 MA (q_a~3.4) and 2.5MA (q_a~2.9) limiter discharges with B_t=4.8T. The pellet data are shown by closed symbols. The increase in W^{DIA} for the 2.1MA discharges is up to 30% at P_{abs}~10MW as compared to the base lines of gas fuelled discharges. The improvement in W^{DIA} for the 2.5MA discharges are relatively small, because the pellet penetrations are shallower and the SX profiles after the injection do not peak. Figure 12 shows the dependence of W^{DIA} on the penetration depth from the axis measured with the pellet monitor for 2.1 and 2.5 MA discharges. For both sets, four pellet injected and a gas puffed shots with the same P_{abs} of 10MW are included. The differences in the penetration length

for each plot are mainly due to the differences in target plasma conditions and in fuelling efficiency of injected pellets. The stored energy increases drastically when pellets penetrate into the core region (r<30cm), otherwise the stored energy of the pellet shots shows small enhancement relative to the gas fuelled cases. In Fig.12 time evolutions of the SX profiles for the four 2.1 MA discharges are also given. The peaked SX profile corresponding to the distinct improvement in W^{DIA} can be produced only when the pellets penetrate deeply into the plasma.

The enhanced stored energy was also observed for pellet injected discharges heated by ICRF alone or in combination with NB. Figure 13 gives the improved performance for 1.5MA limiter discharges heated by OH, ICRF alone, ICRF(<2MW)+NB(2~5MW) and NB alone. The solid and dashed lines indicate the gas fuelled base line for 2.0 and 1.5 MA gas fuelled discharges. For OH and IC heated discharges the improvement in W^{DIA} is about 30%, and that for combined and NB heating cases is up to 40%. For the IC and IC +NB heated discharges, the improvement was observed only when the ion cyclotron resonant surface was located at the plasma center (corresponding to $B_t(0)$=4.3T). For off-axial heating (r~0.32m, r_s~0.2m) with low power IC of only below ~1MW, increase in W^{DIA} after the pellet injection was drastically suppressed even under the best NB+pellet condition. Figure 14 shows time evolutions of soft-X ray signals for chs. 8-12. Two pellets were injected at t=5.95 and 6 sec. During the ICRF heating phase, the peaking of the soft-X ray profile was suppressed and two inversion radii of the sawtooth like oscillation were observed. The ICRF power was observed to be deposited around ch.9 and ch.10 (r~0.14 ~0.21m) from which the energy was released and the inward and outward heat flux increases the SX signal at r<0.14m (ch.11,12) and r>0.28m (ch.8). The behavior is enlarged in Fig.14. After the ICRF heating phase, the SX signals happen to increase and show the usual sawteeth oscillations. This behavior suggests that the safety factor profile in the central region may be double valued.

The increase in τ_E for the limiter discharges was large compared with that for the lower x-point discharges at q_{eff}>3. This is probably because producible ablation profiles are more favorable for the limiter discharges than for divertor ones, since, for the limiter

configuration, the q=1 resonant radius is larger than that of the lower x-point configuration for the same q_{eff} and the pellet trajectory is closer to the magnetic axis.

5. LIMIT OF THE IMPROVED CONFINEMENT

The enhanced stage of pellet fuelled discharges on JT-60 is terminated and degraded to the gas fuelled level when a large sawtooth recovers or the spatial gradient of the SX emission profile (which is considered to correspond to the pressure profile) reaches a critical value. In all cases the central electron temperature was not changed drastically at the crash as shown in Fig.6. This is because T_e profiles for pellet injected discharges are relatively flat, therefore, local interchange of the central plasma column is not considered to alter the measured $T_e(0)$. In the following sub-sections, the two effects limiting the improved confinement for the pellet fuelled discharges, sawtooth recovery and the pressure gradient, are presented.

5.1 Sawtooth Crash

Figure 15 shows the degradation in W^{DIA} occurs simultaneously with the onset of a sawtooth and the strongly peaked SX-profile is broadened at each sawtooth crash. Fig.15(a) compares traces of W^{DIA} for a pellet fuelled (E7994) and a gas fuelled (E8002) 1.5MA lower-x point discharges with the same NB power of 3.5MW. From t=6.2 sec, W^{DIA} for the pellet shot decreases rapidly to the gas fuelled level. Figure 15(b) shows the time traces of SX emission rate for two chords seeing the center and r~2/3a for E7994. After the pellet injection, sawteeth activities are observed within 0.4 sec, then, no sawtooth but the large continuous m=1 mode is activated and W^{DIA} decreases gradually until t=6.21 sec and the first and the second sawteeth occur at t=6.21 and t=6.29 sec, respectively. At each crash the peaked portion of the SX profile at $r \lesssim r_s$ (Ch.9~Ch.10) is drastically flattened (Fig.15(c)) and W^{DIA} happens to decrease.

The target plasmas for the pellet injection experiments on JT-60 have the sawtooth activity before the injection and the safety factor at the axis q(0) is considered to be less than unity. Figure 16 showing traces of change in the internal inductance for E7994 (a) and E8002 (b) implies the current density profile is broadened by the pellet injection: The trace

configuration, the q=1 resonant radius is larger than that of the lower x-point configuration for the same q_{eff} and the pellet trajectory is closer to the magnetic axis.

5. LIMIT OF THE IMPROVED CONFINEMENT

The enhanced stage of pellet fuelled discharges on JT-60 is terminated and degraded to the gas fuelled level when a large sawtooth recovers or the spatial gradient of the SX emission profile (which is considered to correspond to the pressure profile) reaches a critical value. In all cases the central electron temperature was not changed drastically at the crash as shown in Fig.6. This is because T_e profiles for pellet injected discharges are relatively flat, therefore, local interchange of the central plasma column is not considered to alter the measured $T_e(0)$. In the following sub-sections, the two effects limiting the improved confinement for the pellet fuelled discharges, sawtooth recovery and the pressure gradient, are presented.

5.1 Sawtooth Crash

Figure 15 shows the degradation in W^{DIA} occurs simultaneously with the onset of a sawtooth and the strongly peaked SX-profile is broadened at each sawtooth crash. Fig.15(a) compares traces of W^{DIA} for a pellet fuelled (E7994) and a gas fuelled (E8002) 1.5MA lower-x point discharges with the same NB power of 3.5MW. From t=6.2 sec, W^{DIA} for the pellet shot decreases rapidly to the gas fuelled level. Figure 15(b) shows the time traces of SX emission rate for two chords seeing the center and r~2/3a for E7994. After the pellet injection, sawteeth activities are observed within 0.4 sec, then, no sawtooth but the large continuous m=1 mode is activated and W^{DIA} decreases gradually until t=6.21 sec and the first and the second sawteeth occur at t=6.21 and t=6.29 sec, respectively. At each crash the peaked portion of the SX profile at $r \lesssim r_s$ (Ch.9~Ch.10) is drastically flattened (Fig.15(c)) and W^{DIA} happens to decrease.

The target plasmas for the pellet injection experiments on JT-60 have the sawtooth activity before the injection and the safety factor at the axis q(0) is considered to be less than unity. Figure 16 showing traces of change in the internal inductance for E7994 (a) and E8002 (b) implies the current density profile is broadened by the pellet injection: The trace

for E7994 decreases after the pellet injection and recovers to its initial value at t=5.9 sec, then , keeps almost constant value within 0.3 sec and re-starts to increase at t~6.2 sec (1.4 sec after the pellet injection). At this moment the sawtooth reappears. The calculated classical diffusion time of the field line (τ_R) with a characteristic length of 0.2m (~r_s) and T_e of 1.5 keV (~measured value averaged from t=5.8 to 6.2 sec) is 1.9sec, which is comparable to the recovery time of the sawtooth. Therefore, reconstruction of the current-density profile may explain the recovery of the sawtooth activity which is stabilized by the pellet injection within from 0.5 to 1.5 sec. During the sawtooth-free phase produced by deep penetration of pellets, no mode structure or the strong m=1 mode was observed. The MHD behavior similar to those observed on TFTR OH discharges [11] may be caused by the high pressure due to the pellet injection which saturates growth of the island without field line reconnection and produces continuous m=1 activity [21].

5.2 Pressure Gradient

For some discharges with relatively high P_{abs} of 10~15MW, the improved stage is terminated under a sawtooth-free condition. Figure 17(a) shows waveforms of SX emission rate for two chords seeing r=0 and r~2/3a for a 2.1MA limiter discharge (E8120) with P_{abs} of 14MW. Figure 17(b) gives time traces of the total radiated power and local radiated power densities at the center $P_{rad}(0)$ and r=80cm P_{rad}(edge) calculated with Abel inverted signal intensities of a bolometer array, N_i XXVI line emission rate, W^{DIA} and $\bar{n}_e$ (r=0.7a). In the increasing portion of the central SX signal, no sawtooth activity is observed. After the collapse of the SX signal, $P_{rad}(0)$ decreases, P_{rad}(edge) increases, $\bar{n}_e$(0.7a) slightly increases and W^{DIA} decreases. The N_i XXIV line which is considered to be emitted from the central core dose not change drastically as compared to the SX signal but decreases gradually with the reduction in the central density. The result means that the contribution of the heavy impurities to the signal intensity of the SX emission is weak. The calculated power density of the NB deposited at the center is 0.5MW/m^3 which is about 5 times larger than $P_{rad}(0)$ of 0.09MW/m^3, therefore, the rapid flattening of the SX profile cannot be related to the radiation collapse. These behaviors imply the peaked density profile is broadened by the MHD collapse. In Fig.17(a), a large m=1 activity occurs. Sometimes,

large continuous m=1 oscillations were observed during the increasing portion of the central SX emission or no mode structure was detected before and after the SX collapse. The large m=1 mode has not been considered to have large influence on the global confinement of the pellet injected discharges.

In JT-60 pellet fuelled discharges the SX profile well reflects that of the electron pressure. Figure 18 shows the profile of square root of line-integrated soft-X ray intensity and that of the electron pressure n_eT_e measured with the Thomson scattering system for a NB heated 2.1MA limiter discharge (a) and an OH 1.5MA lower x-point discharge (b). The ordinate for the former is adjusted to have the same value with the latter at r=20cm which is the inner most position measurable with the Thomson system. The soft X ray emission rate is roughly proportional to $n_e^2\ T_e^m$ and the m-value changes mainly with the detection system, electron temperature and accumulated impurity species. The SX detection system in JT-60 uses a 250μm thick beryllium window as a SX-filter. For the pellet injected condition on JT-60, Z_{eff}~1.2 and T_e=0.5~2.5keV. If the contribution of heavy impurities for the SX emission rate can be neglected and the main impurity species are oxygen and carbon, m-value is from 1.3 to 2.0 for a parameter regime of Z_{eff}=1.1~2.0 and T_e=0.5~2.5 keV. Therefore, the square root of the SX intensity is in proportion to $n_eT_e^{0.65\sim1}$ which can be considered to give the electron pressure especially for the pellet injected discharges in which the temperature profile is broad and the heavy impurity accumulation is small. In Fig.19(a), the relationship between the plasma stored energy (W^{DIA}) and the volume integrated values of the square root of SX signals, $\sqrt{I_{SX}}$, is shown for I_p=2.1 and 2.5MA limiter and I_p=1.5 and 1.8MA divertor discharges with P_{abs} of 2~25MW. Figure 19(b) shows time evolutions of W^{DIA}, $I_{SX}(r=0)$, $I_{SX}(r=a/2)$ and the volume integrated values of $\sqrt{I_{SX}}$ (closed circles) for a 1.5MA lower x-point discharge. The linear relationship in Fig.19(a) and the agreement of $\int\sqrt{I_{SX}}dV$ with W^{DIA} during the SX profile keeps the peaked shape in Fig.19(b) suggest the SX intensities reflect the plasma pressure and the effects due to the heavy impurity accumulation on the SX emission can be neglected. Figure 20 demonstrates width of the peaked portion of the SX profile decreases with the safety factor and supports our observation that the pressure profile is peaked inside the characteristic radius r_s.

The trigger of the sawtooth-free flattening of the density profile has not been clear so far, because the current density profile cannot be measured experimentally. An ideal ballooning stability analysis, however, shows that the steep pressure gradient after the pellet injection reaches the ideal high-n ballooning limit and the improved confinement is observed clearly to be limited by a critical value of the pressure gradient. Figure 21 shows the pressure profiles estimated using the SX signals for the series of NB heated 1.5MA lower x-point discharges with P_{abs} of from 2 to 16MW. These discharges has almost the same r_s of ~0.18m which was derived by an inversion analysis (fit on the flux surfaces) of SX signals. Every pressure profile consists of a parabolic shaped bias portion and a central 'cap'. The bias parts increase with P_{abs}, but the caps remain almost unchanged, which can explain that pellet data for the 1.5MA lower x-point discharges in Fig.5(b) locate approximately parallel to the gas fuelled data. Figure 21 also means the pressure gradient just inside the sawtooth inversion radius is limited at a certain value. In Fig.22, the gradient of square root of the SX intensity (~pressure gradient) just before the SX collapse are plotted for 2.1MA limiter and 1.5MA lower x-point discharges. The attached marks S and P correspond to sawtooth and sawtooth-free collapses. In the regime of P_{abs}>10MW, the gradient is kept almost constant even when P_{abs} is increased and the improved stage is terminated by the sawtooth-free collapse. The upper limit of the pressure gradient increases with I_p (Fig.23) and the value $\Delta P/I_p^2$ is approximately constant. From figures 20 and 23, it can be concluded that the improvement in confinement is larger for high-I_p discharges, because the 'cap'-width and the gradient are large for high-I_p and low-q discharges.

As shown in Figs. 5(a) and 11, the improvement at high P_{abs} (15~25MW) were small. The reason has not been clear. Figure 24 indicates pressure profiles for 2.1MA limiter and 1.8MA lower x-point discharges estimated when the stored energy takes its maximum. E8115 and E8008 are shots with relatively high P_{abs} of 14MW and 25MW, respectively, and the improvement in W^{DIA} for these were small as shown in Figs. 5 and 11. The pressure profiles for these two discharges are not peaked around the axis and are degraded 0.2~0.3 sec after the pellet injection which is faster than other well improved discharges with medium P_{abs}.

5.3 ACHIEVED CONFINEMENT REGIME

Figure 25 is the Lawson diagram on which data from pellet injected discharges are indicated with large closed circles. The maximum value of the product $n_e(0)\tau_E(a)T_e(0)$ of the pellet discharge is $6.8\times10^{19}m^{-3}$seckeV in a NB heated I_p=2.5MA limiter discharge ($n_e(0)=1.2\times10^{20}m^{-3}$, τ_E=0.2sec, $T_e(0)$=2.8keV and P_{abs}=10MW) where $T_i(0)$ and $n_e(0)$ are considered to be equal to $T_e(0)$ and $n_e(0)$, respectively, since the measured Z_{eff} is smaller than 1.1 and high-density with low-temperature makes the energy equipartition time shorter than several msec. The achieved value of the fusion product exceeds those previously obtained on JT-60 at I_p=3.1MA. Lawson numbers achieved in 1.5MA lower-x point OH discharges ($n_e(0)=1.2\times10^{20}m^{-3}$ and τ_E=0.4sec) also exceeded previously obtained values. Figures 26 (a) and (b) demonstrate the extended density limit for the JT-60 operation by the pellet injection. In each figure, open and closed symbols correspond to the divertor and limiter discharges and the gas and the pellet fuelled discharges are given by circles and triangles. For the pellet discharges, the plotted values are those just after the pellet injection. The allowable density regime was extended by 50~100% , this may be because the power balance in the outer region of the plasma is not deteriorated even at the high average density due to the centrally peaked density profile produced by the pellet injection.

6. SUMMARY

Improved energy confinement for additionally heated JT-60 limiter and lower x-point discharges have been obtained with hydrogen pellet injection. Energy confinement time was enhanced up to 40% relative to usual gas fuelled discharges at the medium NB or NB+ICRF heating power level of <15MW for which the strongly peaked electron density profile with $n_e(0)/\langle n_e\rangle<5$ and $n_e(0)<2.0\times10^{20}m^{-3}$ was sustained within 0.5 sec after a series of pellet injection. Achieved values of $n_e(0)T_e(0)\tau_E(a)$ ($<6.8\times10^{19}m^{-3}$sec keV) at I_p=2.5MA exceeded those previously obtained on JT-60 at I_p=3.1MA. The improved discharges are characterized by the pressure profile strongly peaked around the magnetic axis and degraded when a large sawtooth reappears or the pressure gradient may reach a critical

5.3 ACHIEVED CONFINEMENT REGIME

Figure 25 is the Lawson diagram on which data from pellet injected discharges are indicated with large closed circles. The maximum value of the product $n_e(0)\tau_E(a)T_e(0)$ of the pellet discharge is $6.8\times10^{19}m^{-3}$seckeV in a NB heated I_p=2.5MA limiter discharge ($n_e(0)=1.2\times10^{20}m^{-3}$, τ_E=0.2sec, $T_e(0)$=2.8keV and P_{abs}=10MW) where $T_i(0)$ and $n_e(0)$ are considered to be equal to $T_e(0)$ and $n_e(0)$, respectively, since the measured Z_{eff} is smaller than 1.1 and high-density with low-temperature makes the energy equipartition time shorter than several msec. The achieved value of the fusion product exceeds those previously obtained on JT-60 at I_p=3.1MA. Lawson numbers achieved in 1.5MA lower-x point OH discharges ($n_e(0)=1.2\times10^{20}m^{-3}$ and τ_E=0.4sec) also exceeded previously obtained values. Figures 26 (a) and (b) demonstrate the extended density limit for the JT-60 operation by the pellet injection. In each figure, open and closed symbols correspond to the divertor and limiter discharges and the gas and the pellet fuelled discharges are given by circles and triangles. For the pellet discharges, the plotted values are those just after the pellet injection. The allowable density regime was extended by 50~100% , this may be because the power balance in the outer region of the plasma is not deteriorated even at the high average density due to the centrally peaked density profile produced by the pellet injection.

6. SUMMARY

Improved energy confinement for additionally heated JT-60 limiter and lower x-point discharges have been obtained with hydrogen pellet injection. Energy confinement time was enhanced up to 40% relative to usual gas fuelled discharges at the medium NB or NB+ICRF heating power level of <15MW for which the strongly peaked electron density profile with $n_e(0)/\langle n_e\rangle<5$ and $n_e(0)<2.0\times10^{20}m^{-3}$ was sustained within 0.5 sec after a series of pellet injection. Achieved values of $n_e(0)T_e(0)\tau_E(a)$ ($<6.8\times10^{19}m^{-3}$sec keV) at I_p=2.5MA exceeded those previously obtained on JT-60 at I_p=3.1MA. The improved discharges are characterized by the pressure profile strongly peaked around the magnetic axis and degraded when a large sawtooth reappears or the pressure gradient may reach a critical

value. The peakedness depends strongly on the penetration length of the pellets. Without the peaking of the electron pressure around the plasma core the confinement can be improved, but the enhancement is smaller. In the lower x-point discharges, the improvement was distinct in the low-q ($q<3$) regime probably due to suppression of the sawtooth activity.

ACKNOWLEDGEMENT

The authors would like to gratefully thank Drs. S. Mori, M. Yoshikawa, M.Tanaka S. Tamura, T. Iijima and Y.Shimomura for their continuous encouragement.

value. The peakedness depends strongly on the penetration length of the pellets. Without the peaking of the electron pressure around the plasma core the confinement can be improved, but the enhancement is smaller. In the lower x-point discharges, the improvement was distinct in the low-q ($q<3$) regime probably due to suppression of the sawtooth activity.

ACKNOWLEDGEMENT

The authors would like to gratefully thank Drs. S. Mori, M. Yoshikawa, M.Tanaka S. Tamura, T. Iijima and Y.Shimomura for their continuous encouragement.

REFERENCES

[1] MILORA,S.L., FOSTER,C.A. and EDMONDS,P.H. Phys. Rev. Lett. **42** (1979) 97.

[2] MILORA,S.L., FOSTER,C.A., THOMAS,C.E., BUSH,C.E., WILGEN,J.B., *et al.*, Nucl. Fusion **20** (1980) 1491.

[3] GREENWALD,M., GWINN,D., MILORA,S., PARKER,J., PARKER,R., *et al.*, in *Plasma Physics and Controlled Nuclear Fusion Research* (Proc.10th Int. Conf., London, 1984) Vol.I, (IAEA, Vienna, 1985) ,45. or Phys. Rev. Lett. **53** (1984) 352.

[4] SENGOKU,S., ABE,M., HOSHINO,K., ITOH, K., KAMEARI,A., *et al.*, in *Plasma \ Physics and Controlled Nuclear Fusion Research* (Proc. 10th Int. Conf., London, 1984) Vol.I, (IAEA, Vienna, 1985) ,405.
SENGOKU,S., NAGAMI,M., ABE,M., HOSHINO,K., KAMEARI,A., *et al.*, Nucl. Fusion **25** (1985) 1475.

[5] VLASES,G., GRUBER,O., KAUFMANN,M., BÜCHL,K., HASS,G., *et al.*, Nucl. Fusion **27** (1987) 351.

[6] KAUFMANN,M., BEHRINGER,K., FUSSMANN,G., GRUBER,O., LACKNER,K., *et al.*, in *Plasma Physics and Controlled Nuclear Fusion Research* (Proc.12th Int. Conf., Nice, 1988) IAEA-CN-50/ A-4-2.

[7] KASAI,S., MIURA,Y., HASEGAWA,K. and SENGOKU,S. "Review: Study of Single Pellet Injection Experiments and Development of Pellet Injector in JFT-2M" JAERI-M 87-161 Japan Atomic Energy Research Institute (1987).

[8] GREENWALD,M., BESEN,M., CAMACHO,F., FIORE,C., FOORD,M., *et al.*, in *Plasma Physics and Controlled Nuclear Fusion Research* (Proc. 11th Int. Conf., Kyoto, 1986) Vol.I, (IAEA, Vienna, 1987) ,139.

[9] MILORA,S.L., FOSTER,C.A., Rev. Sci. Instrum. **50** (1979) 482.
COMBS,S.K., MILORA,S.L., FOUST,C.R., *et al.*, Rev. Sci. Instrum. **56** (1985) 1173.
MILORA,S.L., SCHMIDT,G.L., JERNIGAN,T.C., BAYLOR,L.R., COMBS,S.K., in Controlled Fusion and Plasma Heating (Proc. 15th Europ. Conf., Dubrovnik, 1988) Vol.I, p.147.

[10] KAOFMANN.M., Plasma Physics and Controlled Fusion **28** (1986) 1341

[11] SHMIDT,G.L., MILORA.S.L., ARUNASALAM,V., BELL,M.G., BITTER,M., *et al.*, in *Plasma Physics and Controlled Nuclear Fusion Research* (Proc.11th Int. Conf., Kyoto, 1986) Vol.I, (IAEA, Vienna, 1987) ,171.

[12] The JET Team, in *Plasma Physics and Controlled Nuclear Fusion Research* (Proc.12th Int. Conf., Nice, 1988) IAEA-CN-50/ A-4-1.

[13] The JET Team, in *Plasma Physics and Controlled Nuclear Fusion Research* (Proc.12th Int. Conf., Nice, 1988) IAEA-CN-50/ A-1-3.

[14] JT-60 Team, in *Plasma Physics and Controlled Nuclear Fusion Research* (Proc.12th Int. Conf., Nice, 1988) IAEA-CN-50/ A-1-4.

TSUJI,S., AKIBA,M., ANDO,T., ANNOH,K., AOYAGI,T., *et al.*, in *Plasma Physics and Controlled Nuclear Fusion Research* (Proc.12th Int. Conf., Nice, 1988) IAEA-CN-50/ A-5-1.

[15] KAWASAKI,K., HIRATSUKA,H., TAKATSU,H., SHIMIZU.M., ONOZUKA,M., *et al.*, in *Proc. 15th Symposium on Fusion Technology* (Utrecht, 1988) C06 and C07.

[16] NISHITANI,T., "Measurements of the Pellet Ablation Profile on JT-60" to be submitted.

[17] YOSHINO,R. and JT-60 Team, JAERI-M 88-246 (1988).

[18] NAKAMURA,Y., NISHIHARA,H. and WAKATANI,M., Nucl. Fusion **26** (1986) 907

[19] HIRAYAMA,T., SHIMIZU,K., TANI,K., SHIRAI,H. and KIKUCHI,M., "Experimental Transport Analysis Code System in JT-60" JAERI-M 88-043, Japan Atomic Energy Research Institute (1988).

[20] NAITOH,O., *et al.*, to be submitted

[21] DUNLAP,J.L., CARRERAS,B.A., PARE,V.K., HOLMES,J.A., BATES,S.C., *et al.*, Phys. Rev. Lett. **48** (1982) 538.

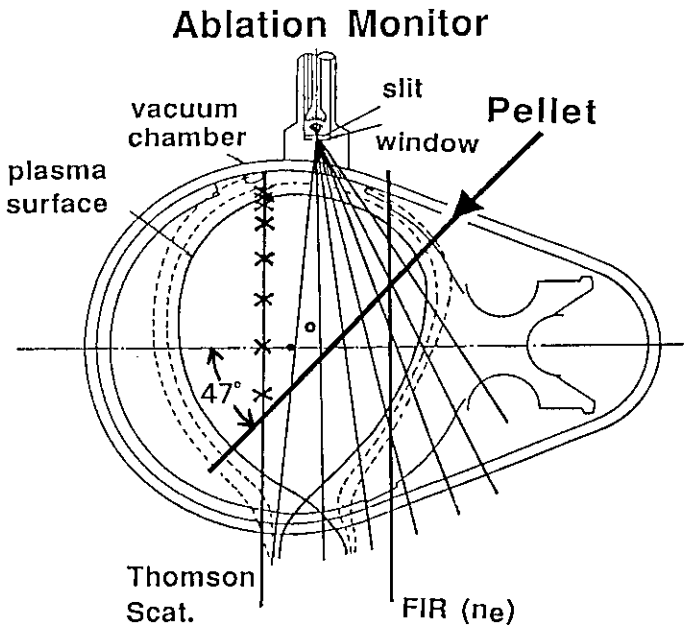

Fig. 1 Lower x-point configuration of a JT-60 plasma. Pellet path, lines of sight of the pellet ablation monitor, chords of a Thomson scattering system (measured points are indicated by ×) and a FIR interferometer are shown.

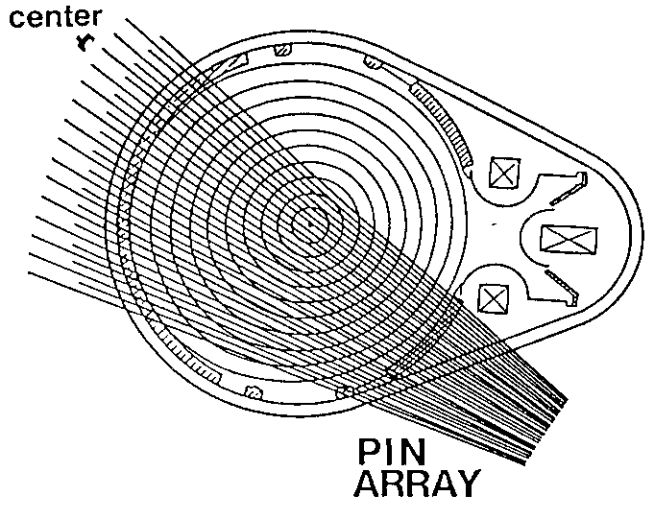

Fig. 2 The limiter configuration and lines of a lower half set of soft-X ray detectors.

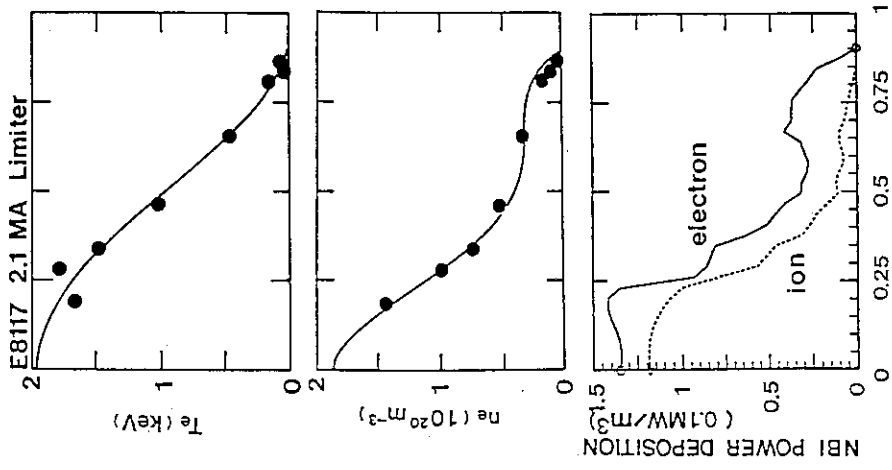

Fig. 4 Achieved electron density and temperature profiles measured with the Thomson scattering system and the power deposition profiles for electron and ion. (NB heated 2.1 MA limiter discharge with P_{abs}~5.4 MW at 0.4 sec after a series of pellet injection.)

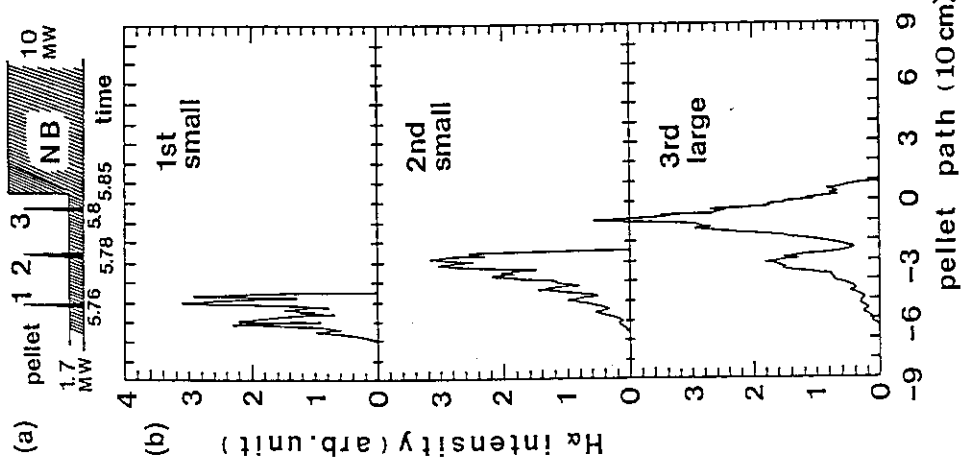

Fig. 3 (a) The pellet injection scenario adopted mainly for the heating experiments and (b) ablation profiles of three pellets for a 1.8 MA lower x-point discharge.

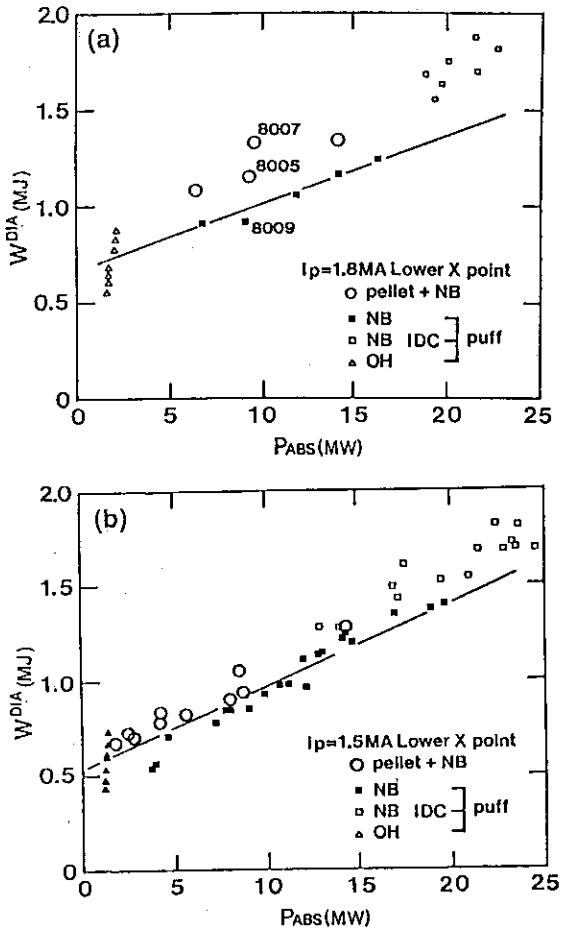

Fig. 5 The relationship between the plasma stored energy W^{DIA} and absorbed power P_{abs} for NB heated 1.8 MA (a) and 1.5 MA (b) lower x-point discharges. The solid lines correspond to the base line of gas fuelled discharges. Data from the improved divertor confinement (IDC) [14] are also plotted.

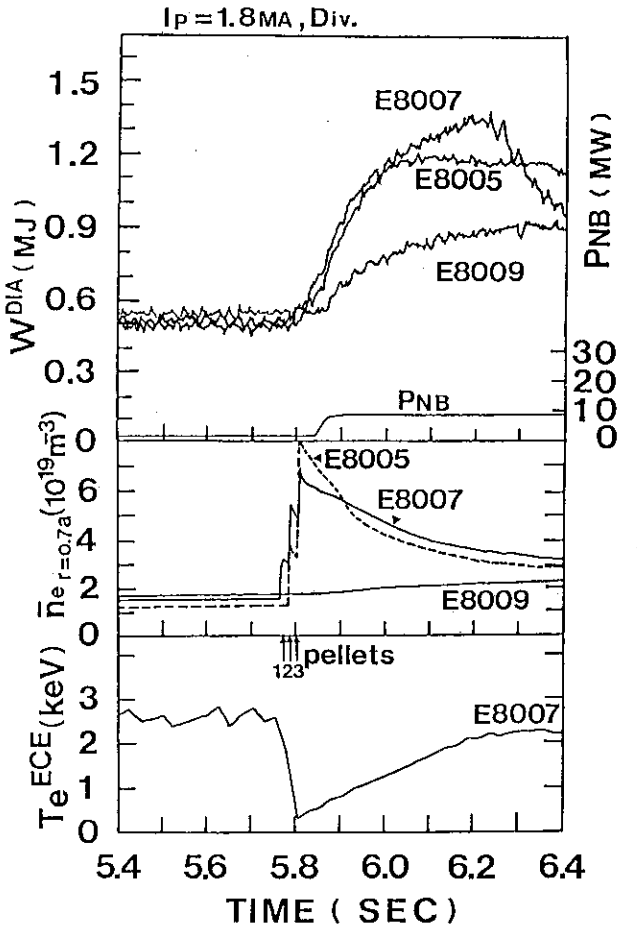

Fig. 6 Time evolutions of W^{DIA} and $\bar{n}_e(r=0.7a)$ for three pellets (E8007), two pellets (E8005) injected and gas fuelled (E8009) 1.8 MA lower x-point discharges and $T_e(0)$ for E8007.

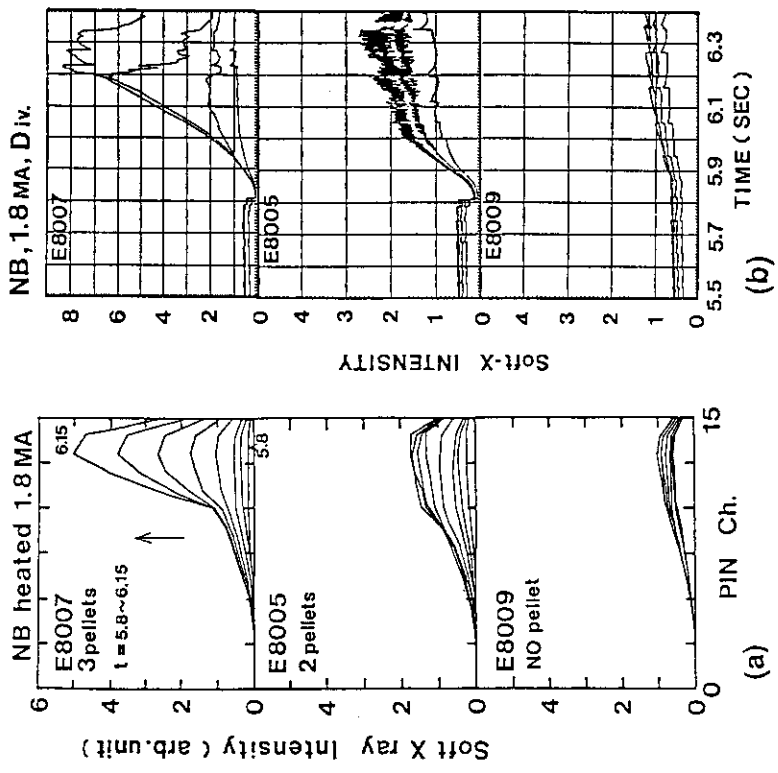

Fig. 8 Signal intensities of soft-X ray for E8007, E8005 and E8009: (a) and (b) show time evolutions of spatial distribution and those for four chords near the magnetic axis.

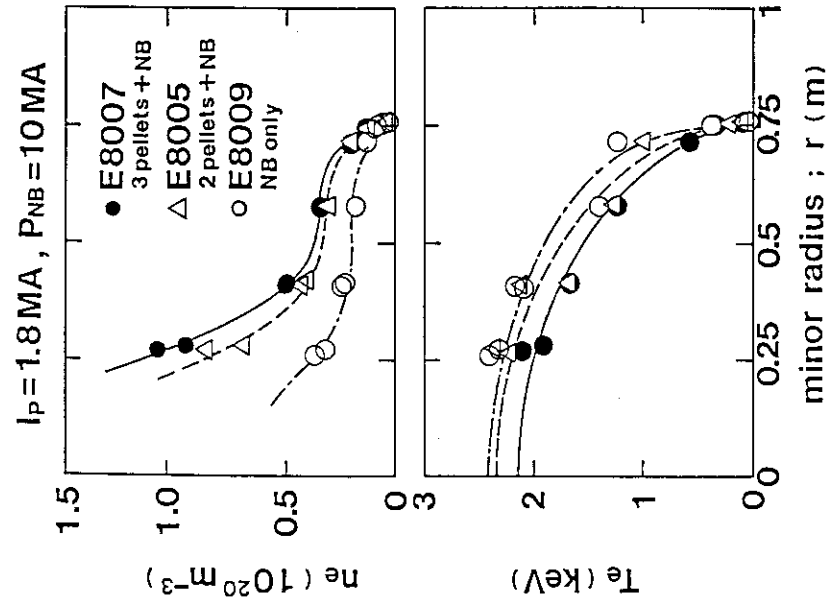

Fig. 7 Profiles of electron density and temperature at 0.4 sec after the pellet injection for E8007 (three pellets), E8005 (two pellets) and E8009 (gas fuelled).

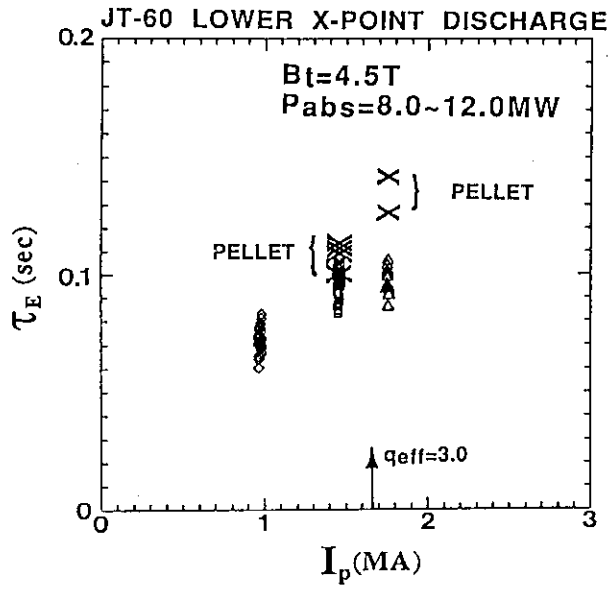

Fig. 9 τ_E for the pellet and gas fuelled lower x-point discharges with B_t=4.5T are plotted as a function of I_p. The improvement due to the pellet injection is distinct at q_{eff}<3.

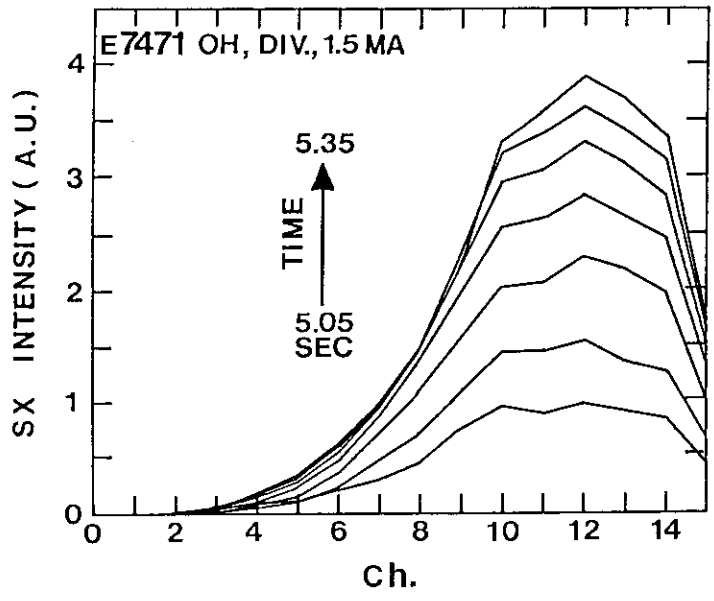

Fig. 10 Time evolution of the SX profile for a 1.5 MA ohmically heated lower x-point discharge. Three pellets are injected at t=4.90, 4.95 and 5.00 sec. The observed profiles are broader than those for NB heated discharges.

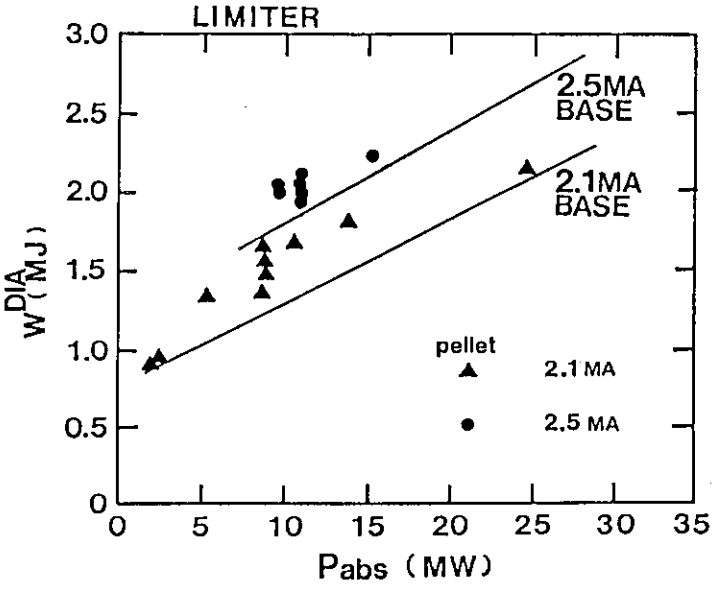

Fig. 11 The relationship between W^{DIA} and P_{abs} for NB heated 2.1 MA (▲) and 2.5 MA (●) limiter discharges. The solid lines correspond to the gas fuelled base lines.

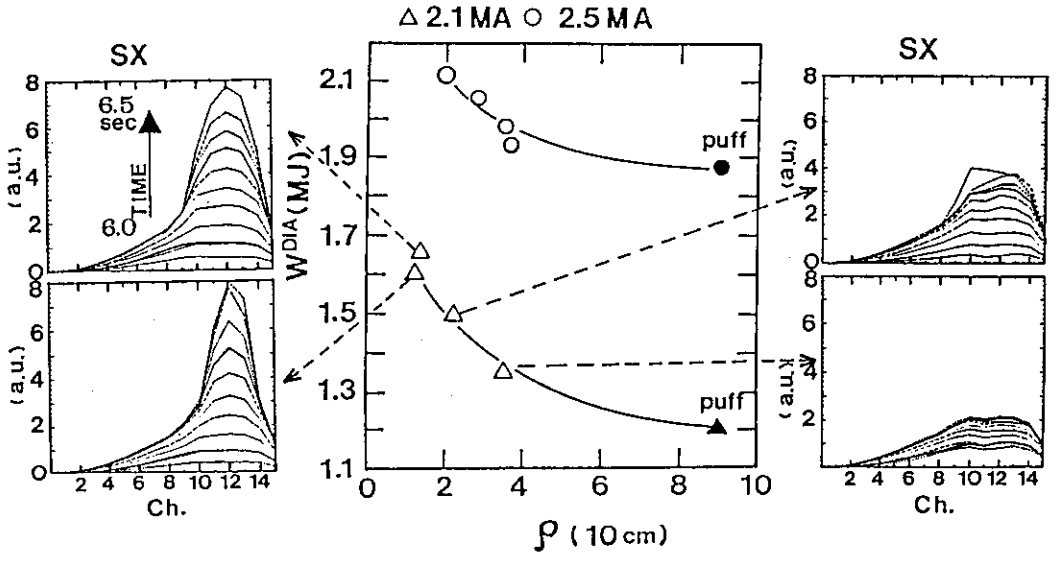

Fig. 12 Dependence of W^{DIA} on the pellet penetration depth from the magnetic axis. Closed symbols correspond to data for gas fuelled discharges. Time evolutions of the SX profiles for the four 2.1 MA pellet injected discharges are also given.

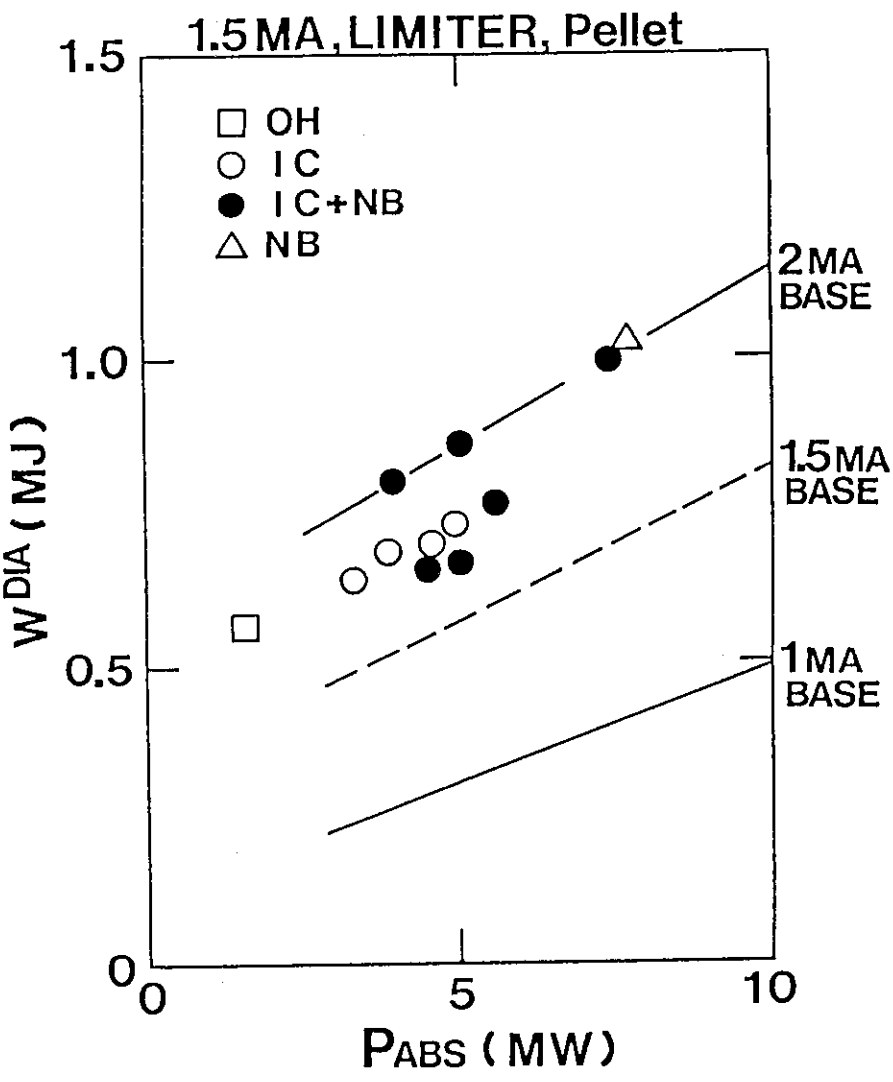

Fig. 13 Improved performance for 1.5 MA limiter discharges heated by OH, ICRF alone, ICRF+NB and NB alone. The base line of 1.5 MA gas fuelled discharges is given by the broken line.

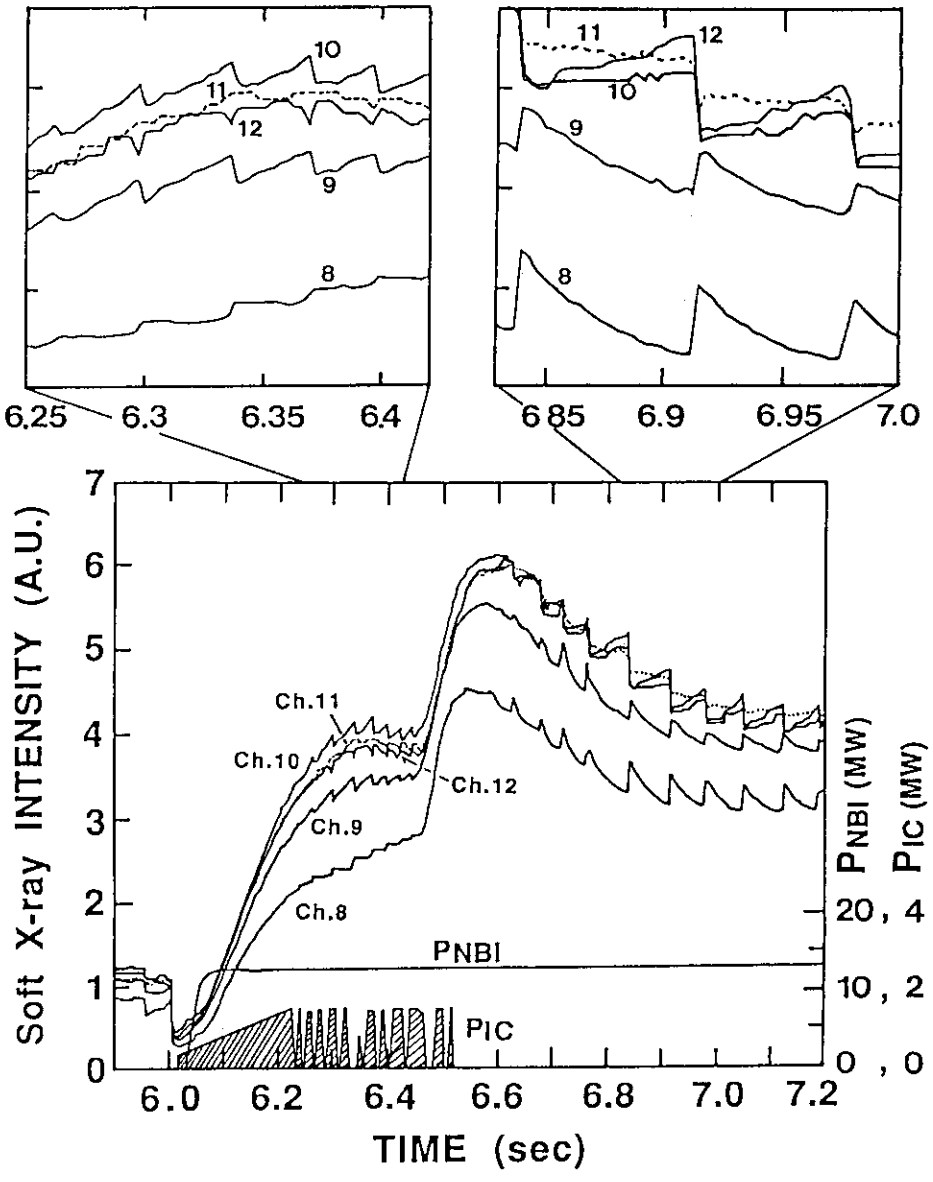

Fig. 14 Time evolutions of soft-X ray signals for a IC and NB heated 2.1 MA limiter discharge. Two pellets were injected at t=5.95 and 6.0 sec. During the ICRF heating, the peaking of the SX profile was suppressed and two inversion radii of the sawtooth oscillation was observed.

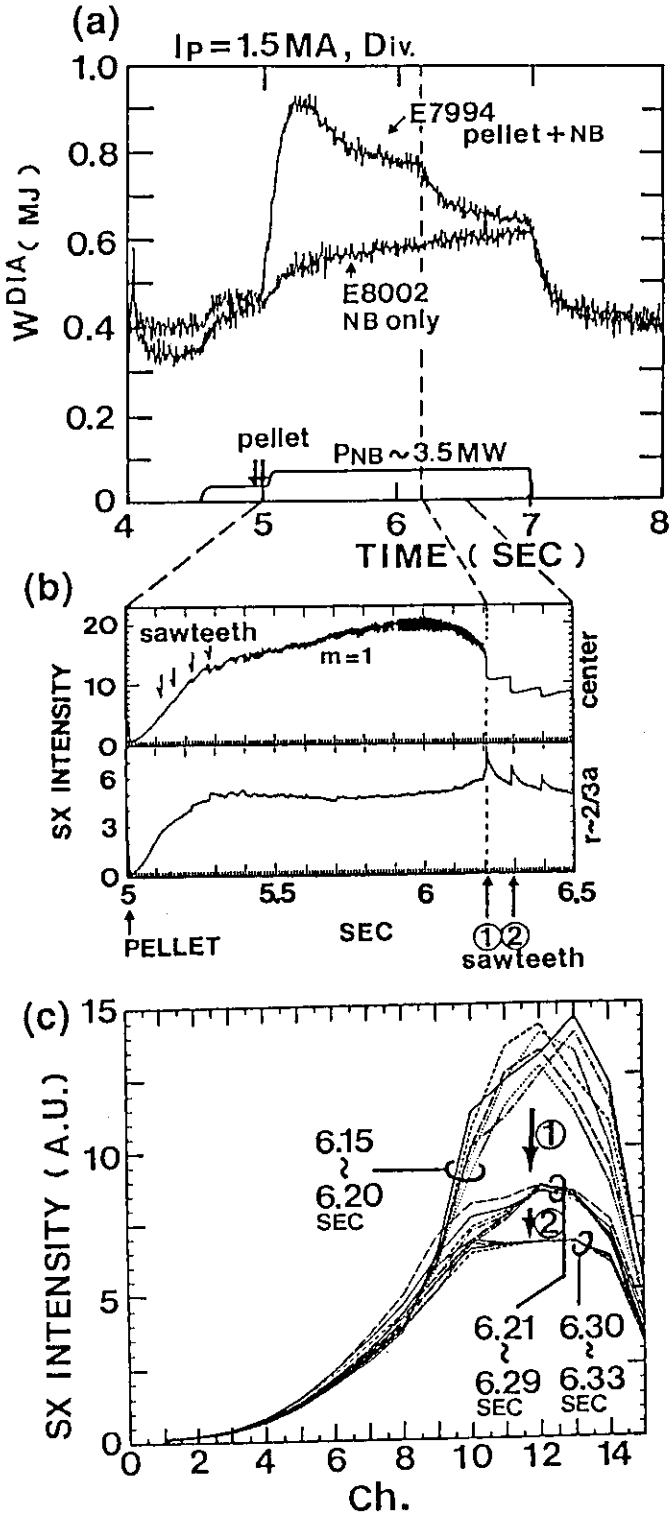

Fig. 15 Degradation in W^{DIA} occurs simultaneously with the onset of a sawtooth. (a) compares traces of W^{DIA} for a pellet fuelled (E7994) and gas fuelled (E8002) discharges with the same NB power. (b) gives time traces of SX emission rate for two chords seeing the center and r~2/3a (E7994). (c) shows that the peaked SX profile is broadened at each sawtooth (E7994).

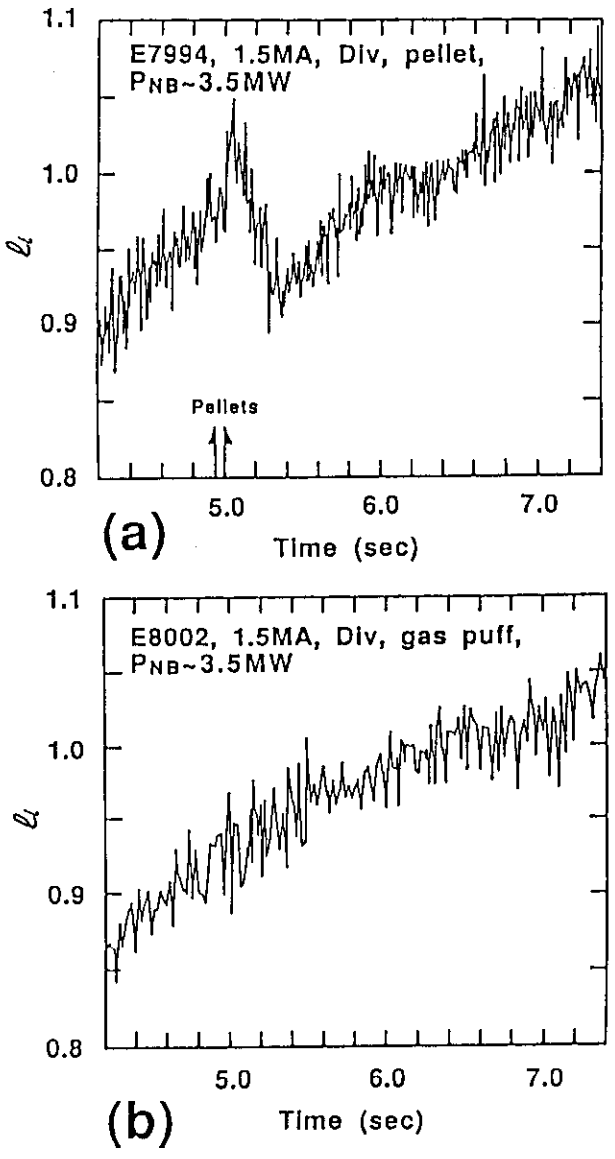

Fig. 16 Time evolution of the internal inductance for E7994 (a) and E8002 (b) given in Fig. 14(a).

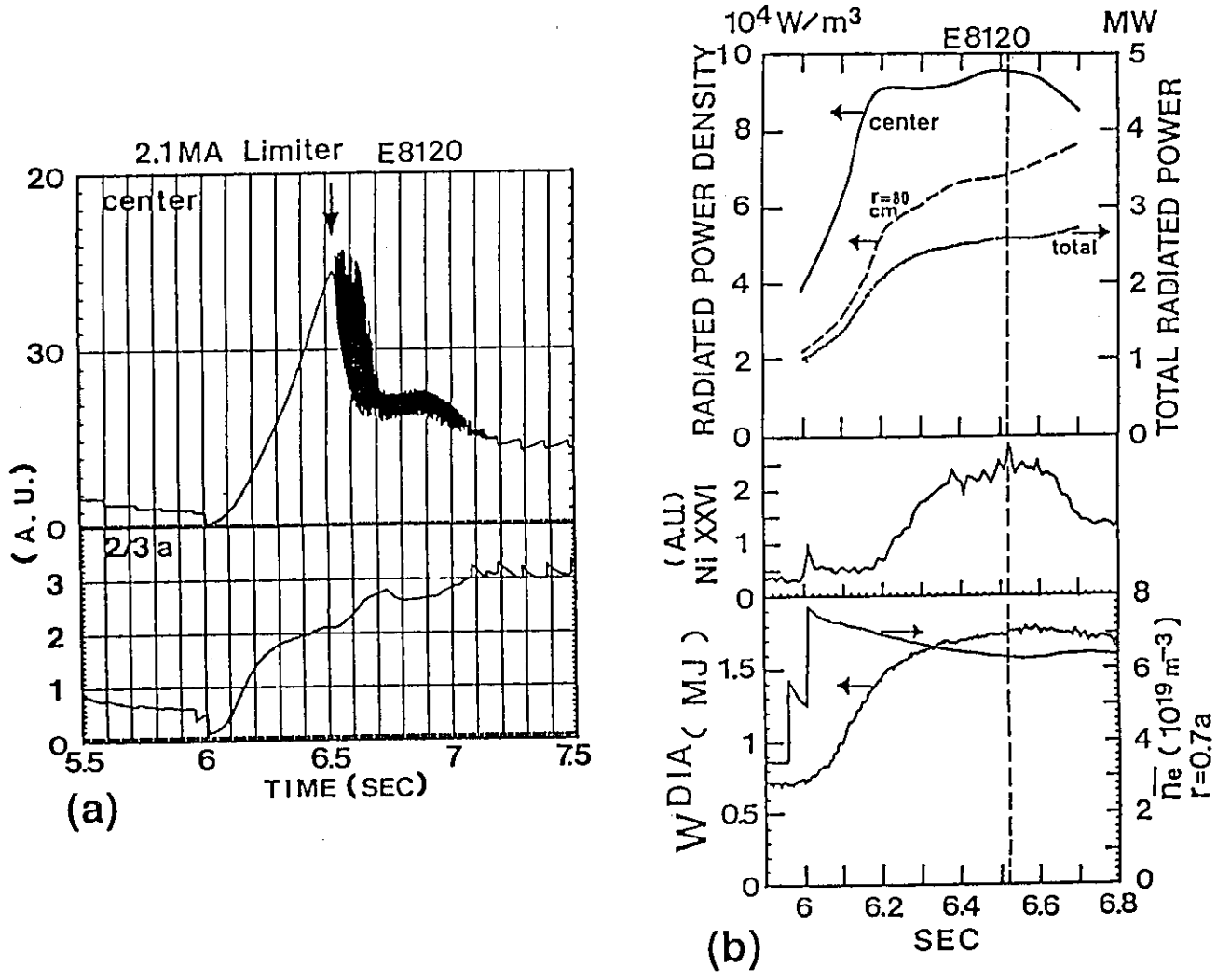

Fig. 17 (a) shows waveforms of SX emission rate for two chords seeing r=0 and r~2/3a for a 2.1 MA limiter discharge with P_{abs} of 14 MW (E8120). (b) gives time evolutions of the total radiation power and local radiated power densities at the center and r=80 cm, NiXXVI line emission, W^{DIA} and $n_e(0.7a)$ for E8120.

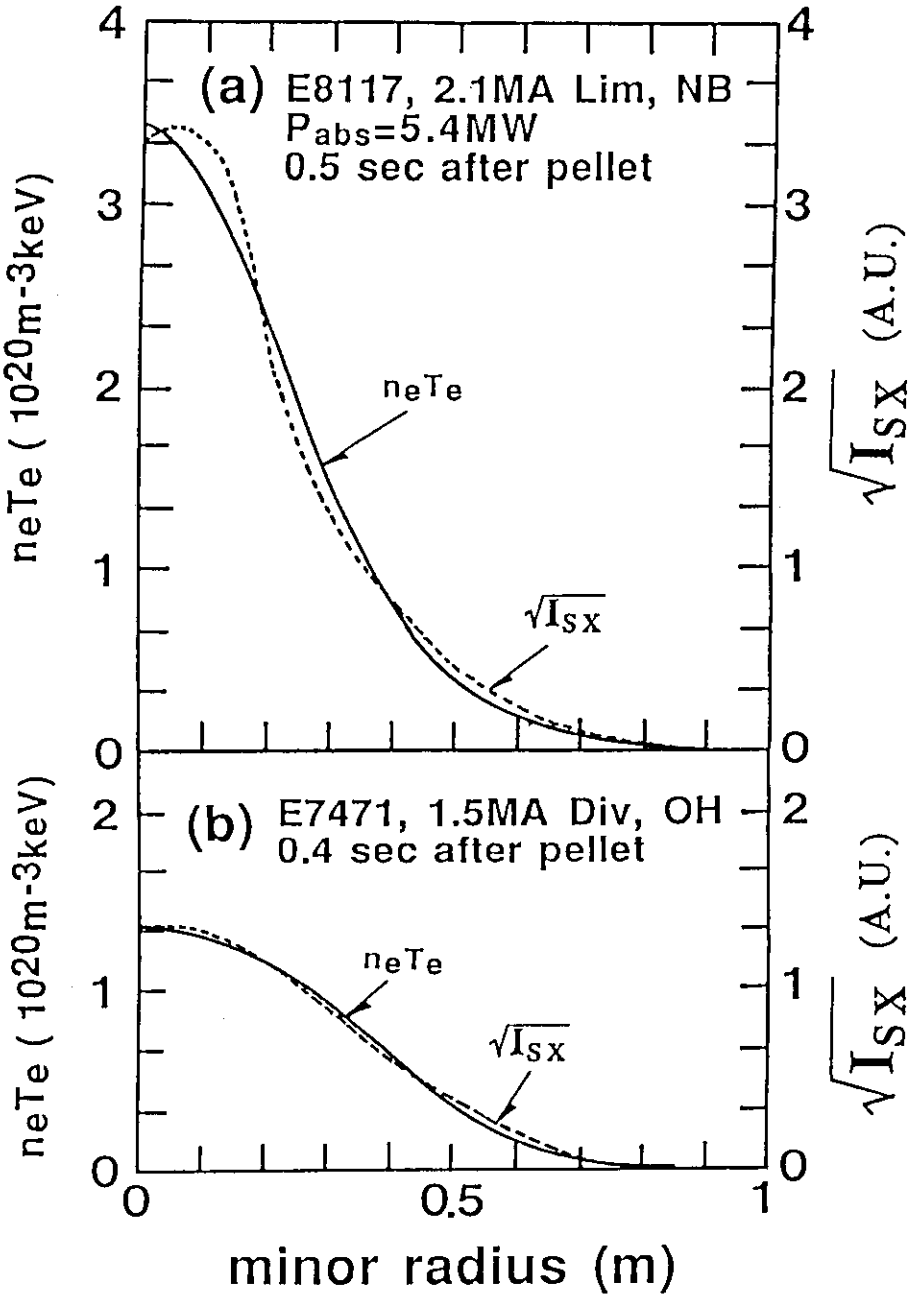

Fig. 18 The figure compares the profile of square root of line-integrated SX intensity and that of the electron pressure n_eT_e measured with the Thomson scattering system for a NB heated 2.1 MA limiter discharge (a) and OH 1.5 MA lower x-point discharge (b).

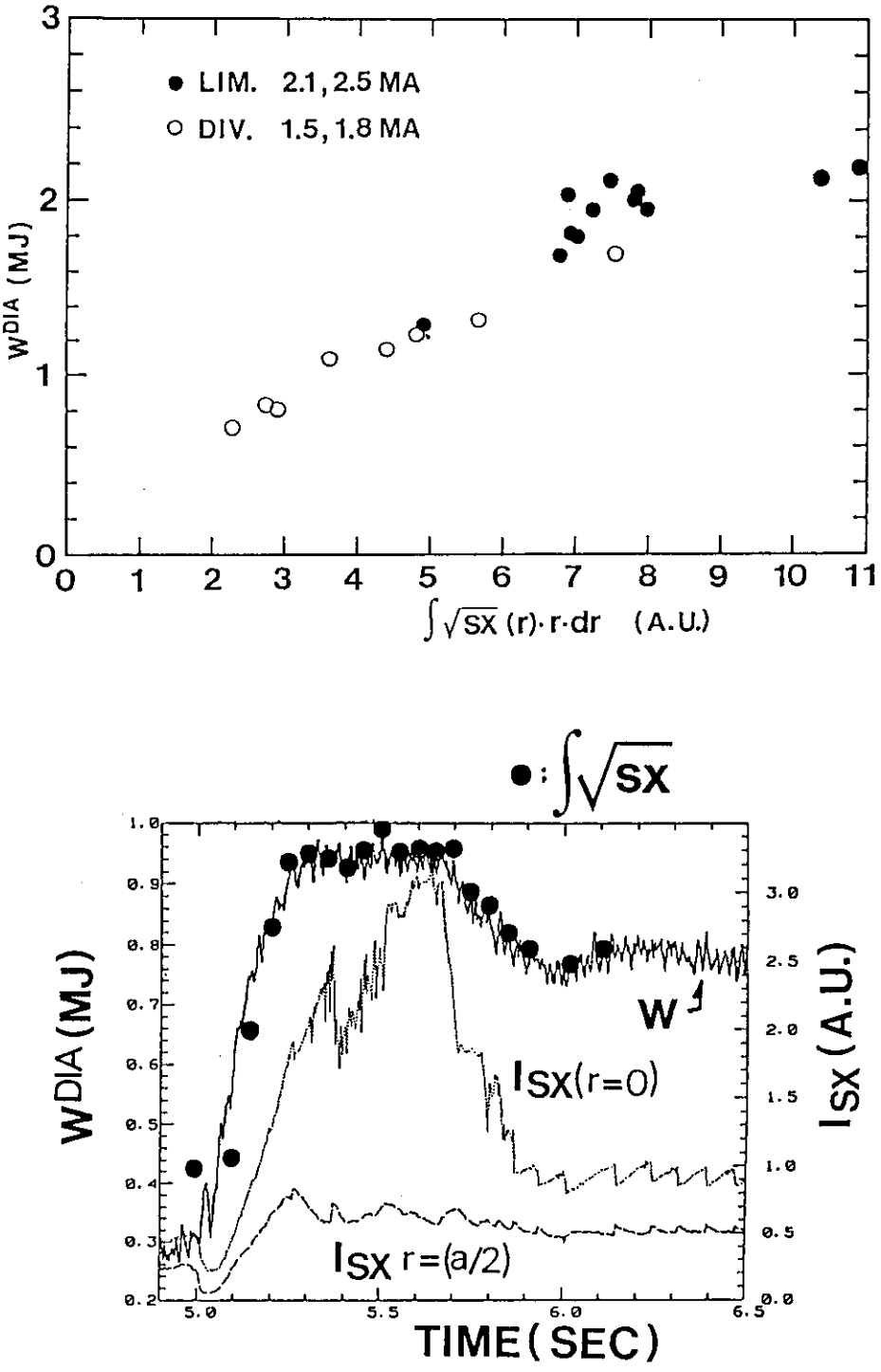

Fig. 19 (a) The relationship between the plasma stored energy and the volume integrated values of the square root of SX signals for 2.1 and 2.5 MA limiter and 1.5 and 1.8 MA lower x-point discharges with Pabs of 2~25 MW and (b) time evolutions of WDIA, ISX (r=0), SIX (r+a/2) and (closed circles) for a 1.5 MA lower x-point discharge E7974.

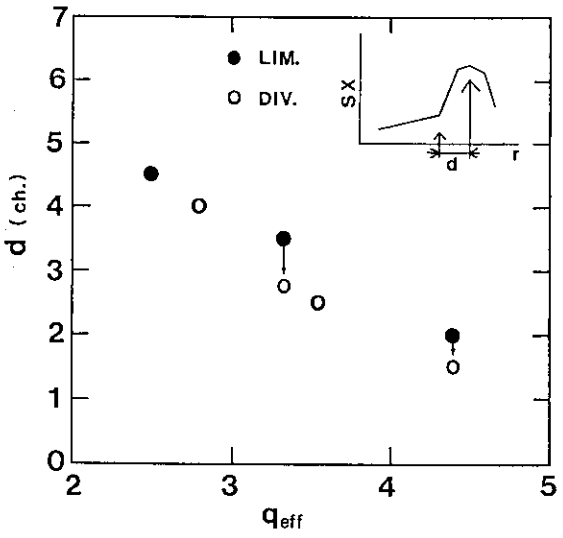

Fig. 20 Width of the peaked portion of the SX profile is shown as a function of the safety factor.

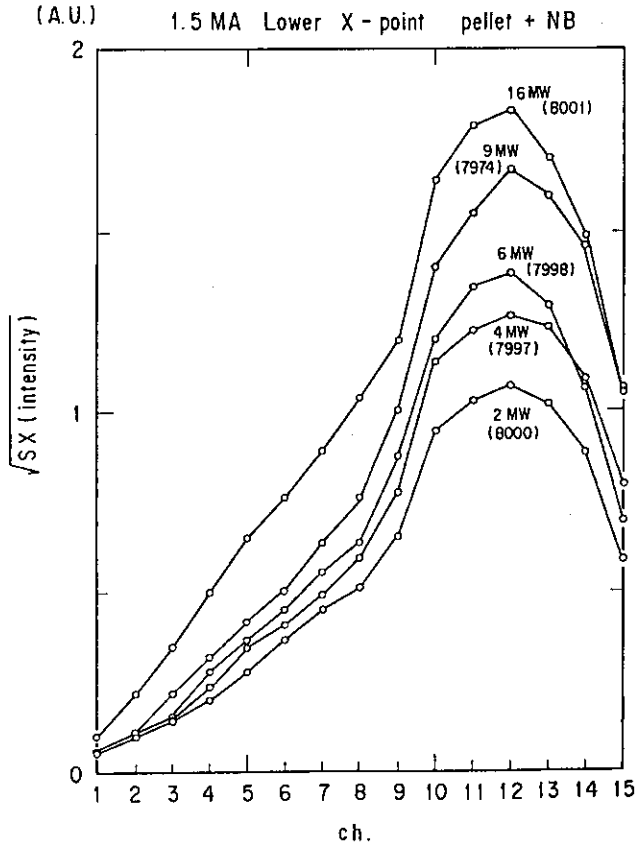

Fig. 21 Pressure profiles estimated with the SX signals for the series of 1.5 MA lower x-point discharges. The pressure gradients just inside the sawtooth inversion radius remain unchanged even with increasing P_{abs}.

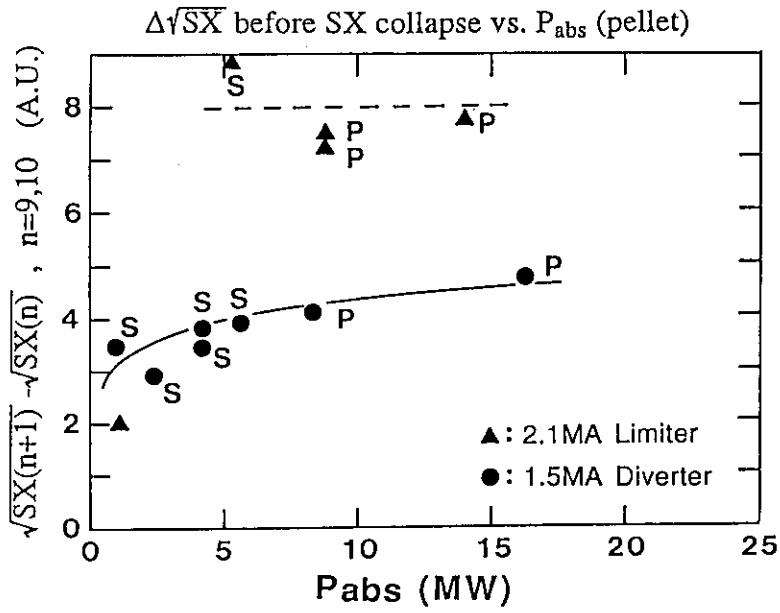

Fig. 22 The maximum gradient of square root of the SX intensity just before the SX collapse for 2.1 MA limiter and 1.5 MA lower x-point discharges as a function of P_{abs}. Attached marks S and P correspond to sawtooth and sawtooth-free collapses.

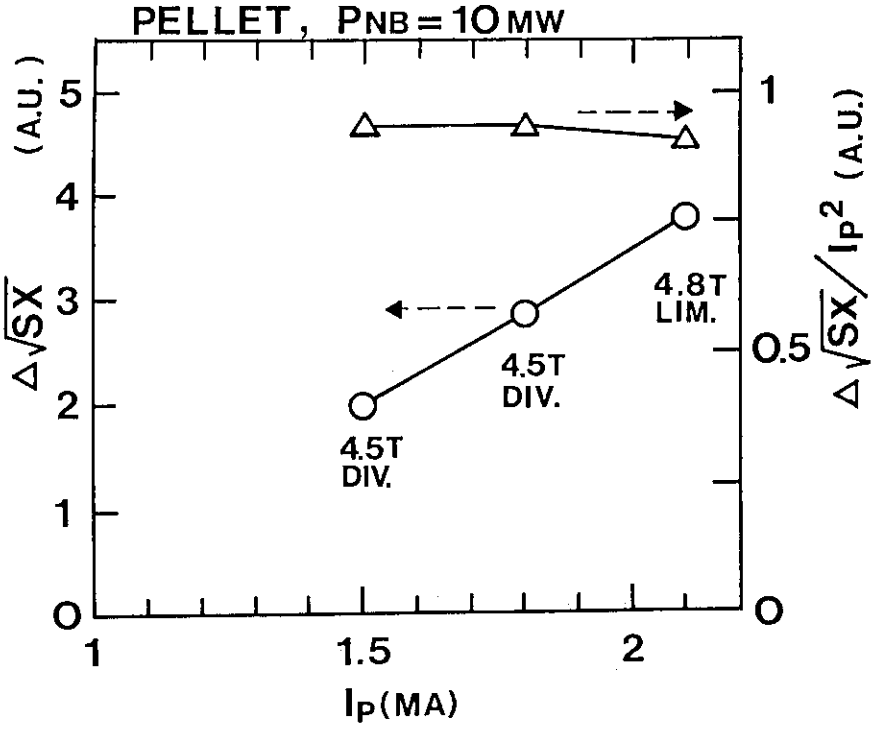

Fig. 23 The upper limit of the pressure gradient estimated with the SX signals for pellet injected discharges with P_{abs} of ~10 MW.

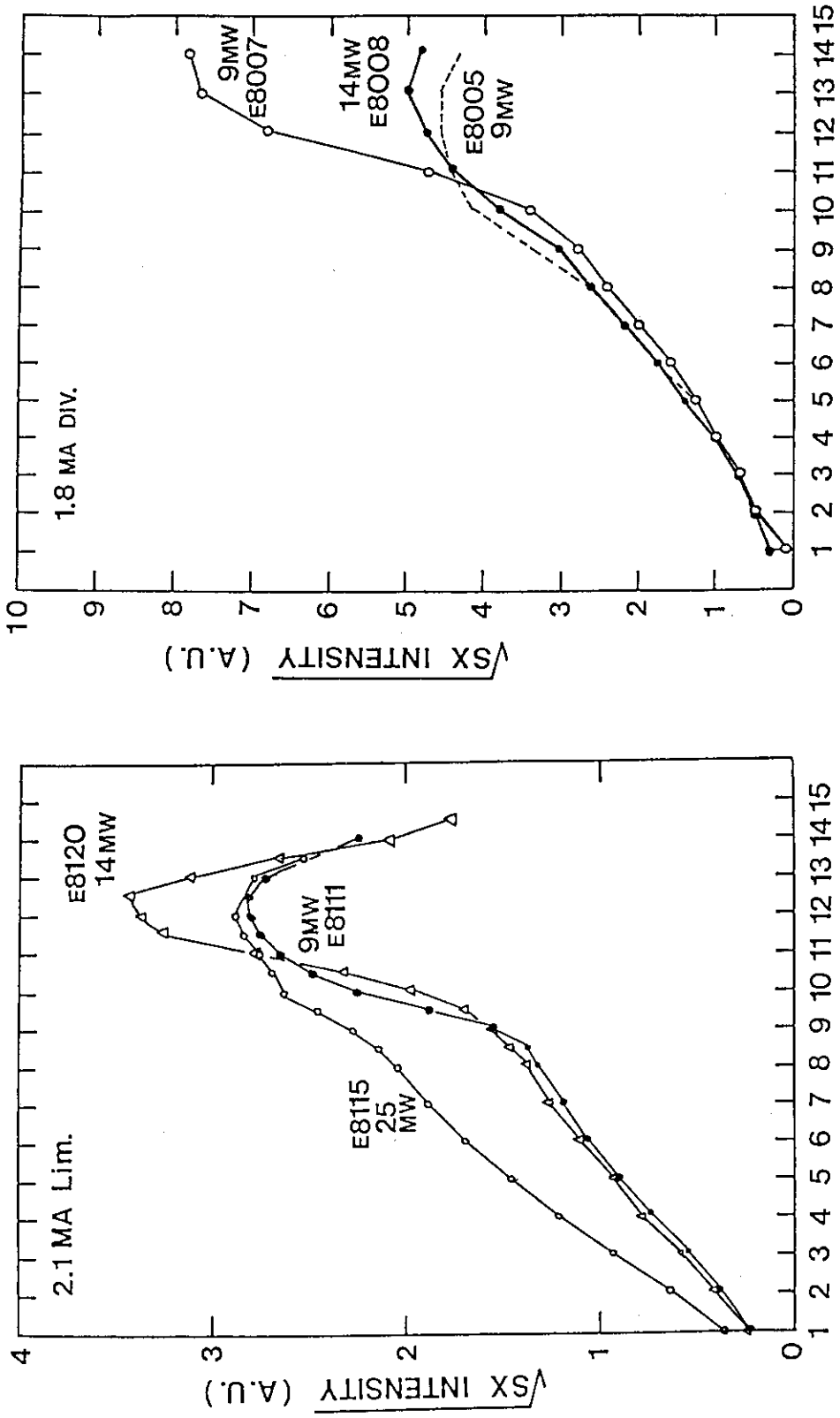

Fig. 24 Pressure profiles for 2.1 MA limiter and 1.8 MA lower x-point discharges at the time when the stored energy takes its maximum. E8115 and E8008 are shots where relatively high NB powers of 25 and 14 MW were injected.

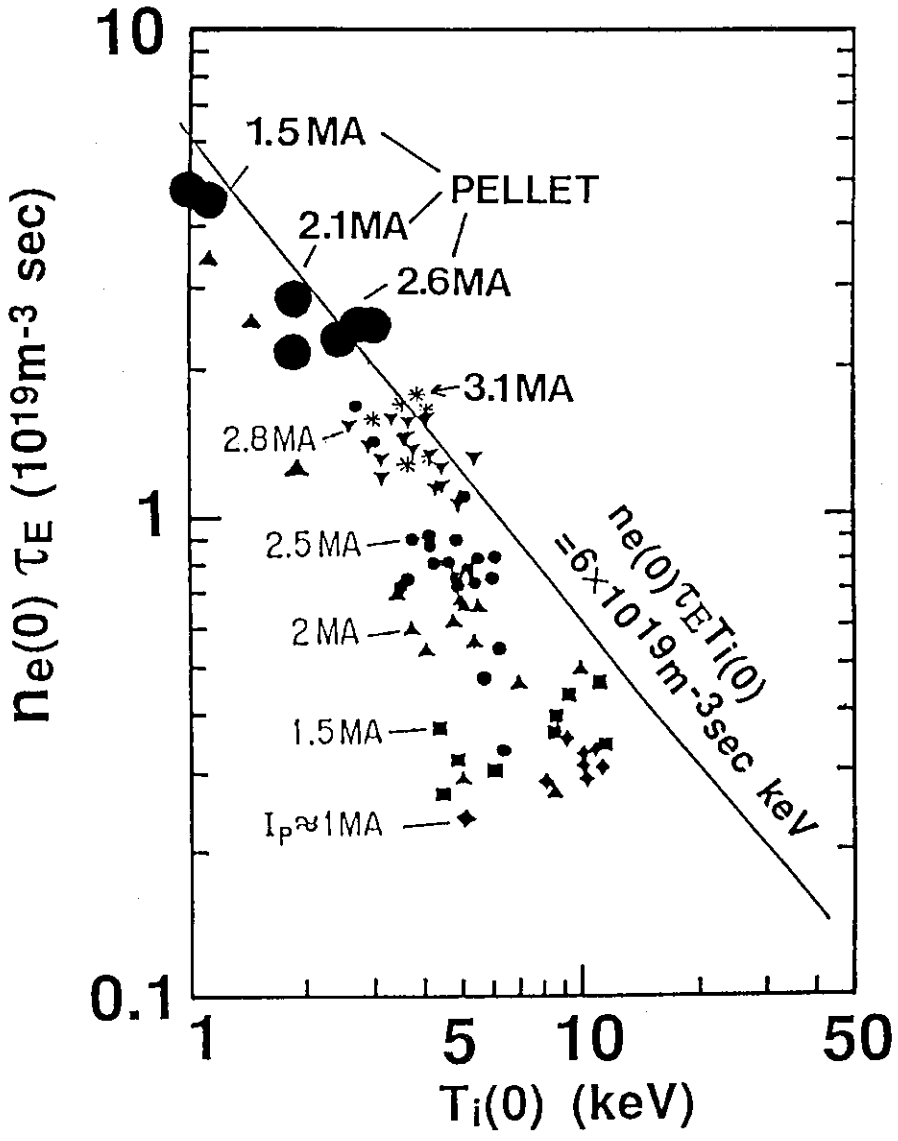

Fig. 25 Lawson diagram for JT-60 plasmas. Data from pellet injected discharges are indicated with large closed circles.

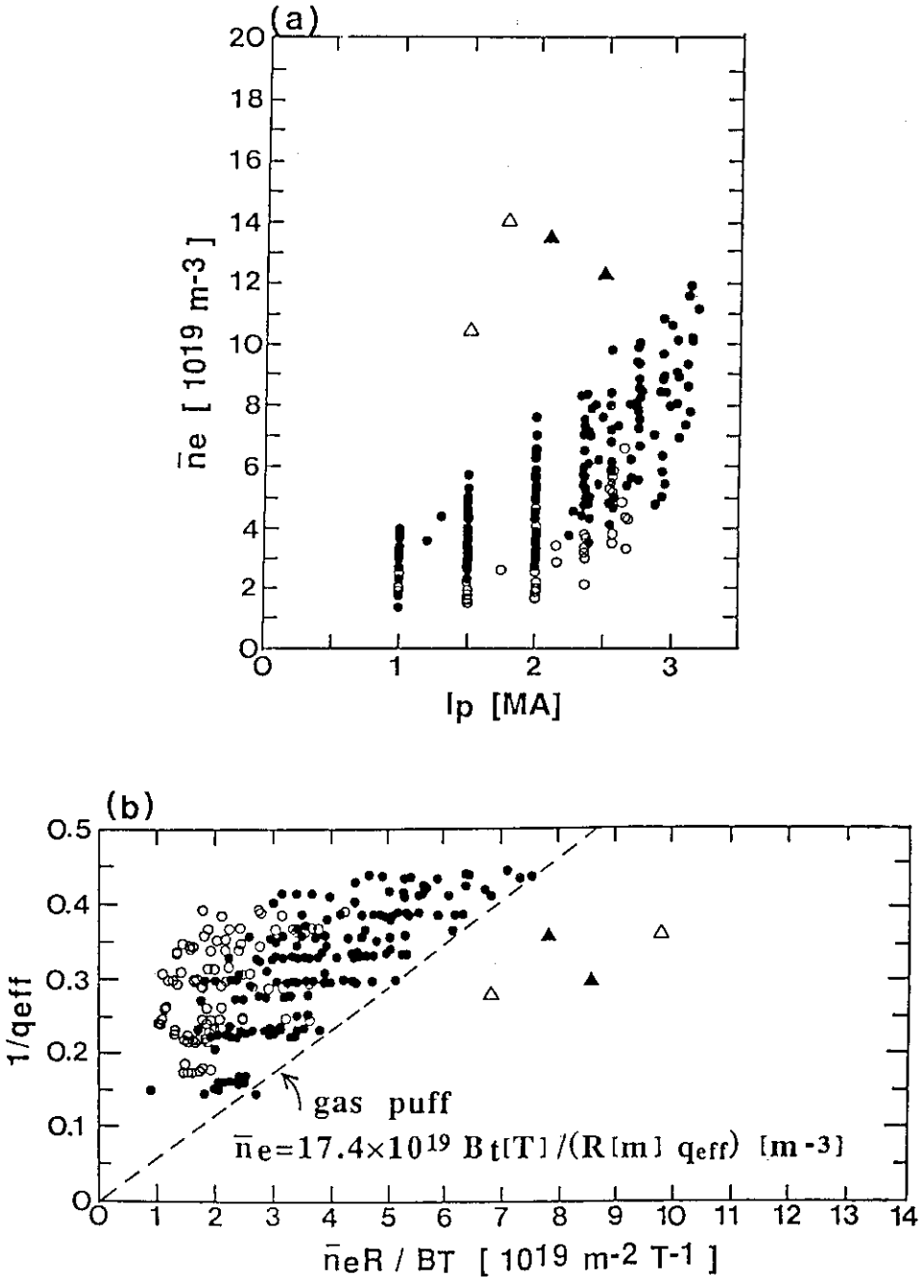

Fig. 26 Extended operation regime for the electron density by the pellet injection. Open and closed symbols correspond to divertor and limiter discharges and gas and pellet fuelled shots are indicated by circles and triangles.